Inorganic Chemistry

pubs.acs.org/IC

Article

Experimental and Computational Study of the Structure, Steric Properties, and Binding Equilibria of Neopentylphosphine Palladium Complexes

Kerry L. Barnett, Monica Vasiliu, Trent H. Stein, Matthew V. Delahay, Fengrui Qu, Deidra L. Gerlach, David A. Dixon,* and Kevin H. Shaughnessy*

Cite This: *Inorg. Chem.* 2020, 59, 5579–5592

Read Online

ABSTRACT: Steric properties of crystallographically and computationally determined structures of linear palladium(0) and square planar palladium(II) complexes of di(*tert*-butyl)neopentylphosphine (P(*t*-Bu)$_2$Np), *tert*-butyldineopentylphosphine (P(*t*-Bu)Np$_2$), and trineopentylphosphine (PNp$_3$) have been determined. Structures of linear palladium(0) complexes show that steric demand increases as *tert*-butyl groups are replaced with neopentyl groups (P(*t*-Bu)$_2$Np < P(*t*-Bu)Np$_2$ < PNp$_3$). In square planar palladium(II) complexes, PNp$_3$ gives the smallest steric parameters, whereas P(*t*-Bu)Np$_2$ has the largest steric demand. The change in the steric demand of PNp$_3$ compared to P(*t*-Bu)$_2$Np and P(*t*-Bu)Np$_2$ results from a significant conformational change in PNp$_3$ depending on the coordination number of the metal. The steric properties of these ligands were also probed by measuring the equilibrium constant for coordination of free phosphine to dimeric [(R$_3$P)Pd(μ-Cl)Cl]$_2$ complexes. Binding equilibria follow the same trend as the steric parameters for square planar complexes with PNp$_3$ having the highest binding constant. In contrast to the normal trend, the neopentylphosphines show increased pyramidalization at phosphorus with increasing steric demand. We hypothesize that this unusual dependence reflects the low back side strain of the neopentyl group, which allows the ligand to be more pyramidalized while still exerting a significant front side steric demand.

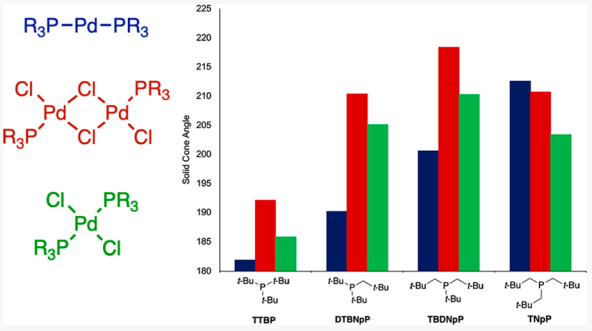

INTRODUCTION

Phosphorus-based ligands represent the predominant class of supporting ligands for homogeneous catalytic processes involving late transition metals. Because phosphorus-based ligands can be synthesized with a nearly infinite variety of substituents, the properties of these ligands can be widely varied to promote desired catalytic reactions. Electronic properties can be varied from strongly σ-donating trialkylphosphines to π-accepting phosphites. Steric properties can similarly be varied over a wide range of cone angles from PMe$_3$ (118°) to P(mesityl)$_3$ (212°). This wide range of steric and electronic variability makes it important to be able to quantify steric and electronic properties to allow ligand properties to be compared. Quantifying steric properties becomes particularly challenging with conformationally flexible ligands that may have different low energy conformations as a function of the structure of the coordinated metal complex.

A number of steric and electronic descriptors have been developed in an effort to quantify the effects of ligands on metal centers in catalyst systems.[1] The Tolman cone angle (θ) was the first quantified description of the steric impact of ligands and remains a widely used steric descriptor (Figure 1).[2] The Tolman cone angle is based on the least sterically demanding conformation of a ligand, which is not always the lowest energy conformation. Allen's exact cone angle parameter uses Tolman's definition but is based on the low energy conformation of the metal–ligand complex.[3] To address ligands with nonsymmetric steric profiles, the solid cone angle (Ω) was developed.[4] The solid cone angle is derived from the area of the shadow projected by the ligand atoms on a sphere surrounding the metal, which can be converted to a vertex angle analogous to the Tolman cone angle.

The percent buried volume (%V_{bur}) parameter developed by Nolan et al. measures the percentage of a sphere occupied by the ligand.[5] The %V_{bur} has gained popularity as it can be calculated with a simple web interface and handles nonsymmetric ligands, such as NHCs and chelating ligands, more

Received: January 27, 2020
Published: April 9, 2020

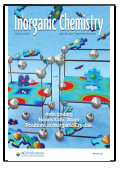

https://dx.doi.org/10.1021/acs.inorgchem.0c00266
Inorg. Chem. 2020, 59, 5579–5592

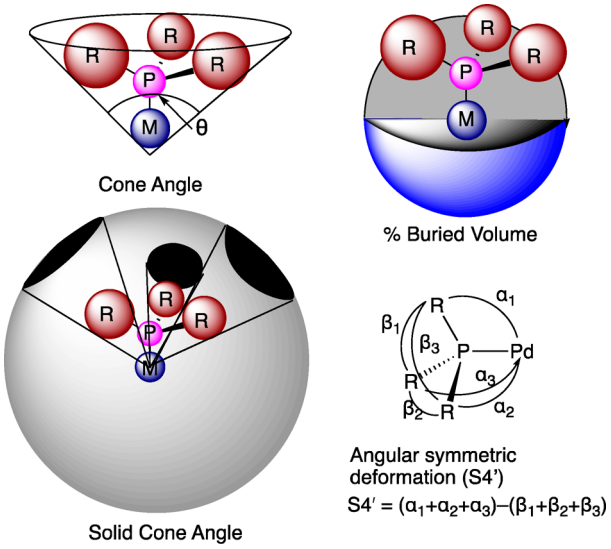

Figure 1. Steric descriptors of phosphine ligands.

easily than the cone angle description. Orpen et al. described the angular symmetric deformation parameter (S4′) as an easily measured steric descriptor. S4′ is defined as the difference between the sum of the M−P−C angles (α) and P−C−C angles (β).[6] This parameter provides a measure of the pyramidalization of the phosphorus center and is found to inversely correlate with the Tolman cone angle.[7]

The Tolman electronic parameter (χ) based on the symmetric CO stretch of $LNi(CO)_3$ complexes is the basis for the majority of reported ligand electronic properties.[2b,8] Because of the toxicity of $Ni(CO)_4$; molybdenum, iridium, and rhodium carbonyl complexes have been correlated with the original Tolman scale.[9] Other electronic parameters that have been applied to analyzing phosphine ligands include the pK_a of phosphonium ions, proton affinity, calculated charge on phosphorus, and the HOMO energy level of the phosphine.[1b,10]

Our group has been interested in phosphines containing conformationally flexible neopentyl substituents, such as di-*tert*-butylneopentylphosphine ($P(t\text{-Bu})_2Np$; Figure 2), *tert*-

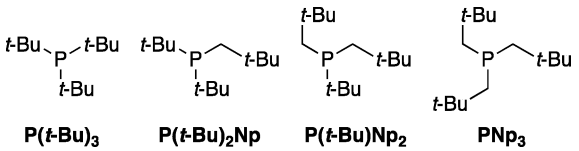

Figure 2. Structures of $P(t\text{-Bu})_3$ and neopentyl phosphines

butyldineopentylphosphine ($P(t\text{-Bu})Np_2$), and trineopentylphosphine (PNp_3). $P(t\text{-Bu})_2Np$ provides active catalysts for a variety of traditional palladium-catalyzed cross-coupling reactions of aryl bromides and chlorides.[11] Interesting differences between catalysts derived from $P(t\text{-Bu})_2Np$ and PNp_3 have been observed in these reactions. In the Heck coupling of cyclic alkenes, $P(t\text{-Bu})_2Np$ and PNp_3 afford catalysts with orthogonal olefin product selectivity.[12] The $P(t\text{-Bu})_2Np$/Pd catalyst system is not effective for cross-coupling of sterically demanding substrates. In contrast, the catalyst derived from palladium and PNp_3 is effective at coupling sterically demanding aryl halides.[11d,13] The ability of PNp_3-derived catalysts to couple sterically demanding substrates has been ascribed to its conformational flexibility compared to more rigid ligands like $P(t\text{-Bu})_2Np$ and $P(t\text{-Bu})_3$.[13b,14]

The replacement of *tert*-butyl substituents with neopentyl groups introduces a degree of conformational flexibility into the ligand. The steric demand of the neopentyl substituent is expected to vary depending on the M−P−C−C dihedral angle (Figure 3). When the neopentyl group is *syn* coplanar with the

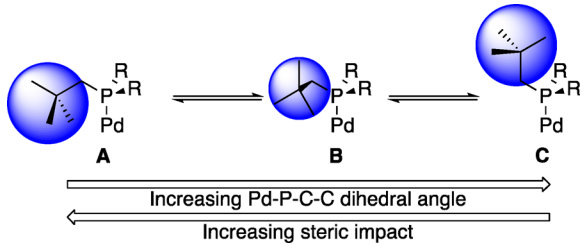

Figure 3. Potential effect of the change in the Pd−P−C−C dihedral angle of neopentylphosphines on the ligand steric demand.

P−Pd bond (A), it has maximum steric impact. As the Pd−P−C−C dihedral angle increases, the steric demand is expected to decrease with a minimal value in the *anti* conformation (C). This flexibility is analogous to that observed in phosphite ligands.[15] Analysis of crystal structures shows that $P(OMe)_3$ can have cone angles ranging from 103 to 139°, with the majority of experimental structures having much larger values than the Tolman cone angle of 107°.[16]

The steric and electronic properties of the neopentylphosphine ligands have been previously analyzed using experimental and computational data.[11a,b] Solid cone angles based on calculated LPd(0) complexes showed that replacing *tert*-butyl groups with neopentyl substituents increased the ligand steric demand. The low energy conformations for these complexes have small Pd−P−C−C dihedral angles for the neopentyl substituents (conformation A, Figure 3). We have since reported crystal structures of square planar palladium(II) complexes with these ligands, that have conformations of type B and C.[11c,f,13b,14] On the basis of these observations, we hypothesized that the steric parameters determined for LPd(0) may not be relevant to the square planar palladium(II) complexes that are key catalytic intermediates in cross-coupling reactions. In particular, PNp_3 undergoes a large conformational change depending on the metal coordination number, which might be expected to significantly affect the steric properties of this ligand.

In this work, a detailed analysis of the structure of the $P(t\text{-Bu})_nNp_{3-n}$ (n = 0−3) has been performed for the ligands coordinated in linear palladium(0) and square planar palladium(II) complexes to determine how coordination number affects the conformation and steric properties of neopentylphosphines. Both types of complexes are relevant to the palladium-catalyzed cross-coupling reaction catalytic cycle involving a Pd(0/II) redox cycle. We report that the steric demand of PNp_3 varies significantly depending on the coordination number of the metal complex, whereas the more rigid $P(t\text{-Bu})_2Np$ has a smaller range of steric effects. The effective steric demand of these ligands was probed by measuring the binding equilibrium for these ligands with $[LPd(\mu\text{-Cl})Cl]_2$ complexes to afford *trans*-L_2PdCl_2.

https://dx.doi.org/10.1021/acs.inorgchem.0c00266
Inorg. Chem. 2020, 59, 5579−5592

RESULTS

Synthesis of $[(R_3P)Pd(\mu\text{-}Cl)Cl]_2$ and *trans*-$(R_3P)_2PdCl_2$ Complexes. The neopentylphosphine palladium complexes were prepared using known procedures to give $[(R_3P)Pd(\mu\text{-}Cl)Cl]_2$ (**1a**–**1c**) and $(R_3P)_2PdCl_2$ (**2a**–**2c**) complexes (Scheme 1).[11f] The complexes are air stable and show no

Scheme 1. Synthesis of $[(R_3P)Pd(\mu\text{-}Cl)Cl]_2$ (1a–1c) and *trans*-$(R_3P)_2PdCl_2$ (2a–2c) Complexes

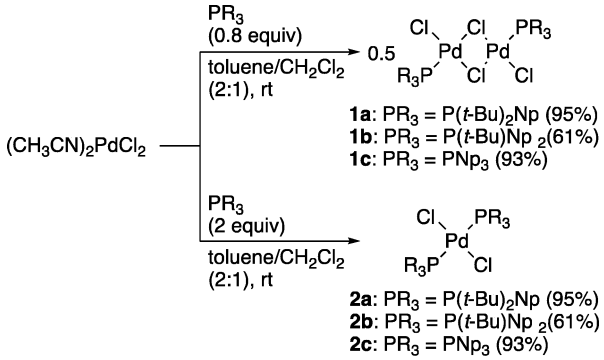

signs of decomposition upon storage in air at ambient temperature for extended periods. In contrast, $[((t\text{-}Bu)_3P)Pd(\mu\text{-}Cl)Cl]_2$ undergoes decomposition by ligand metalation over the course of several days.[17] $((t\text{-}Bu)_3P)_2PdCl_2$ has been reported,[18] but no structural or spectroscopic data have been published for this complex. Our attempts to prepare this complex indicated that it undergoes cyclometalation over the course of several hours in solution.

The ^{31}P NMR chemical shifts for the $[(PR_3)Pd(\mu\text{-}Cl)Cl]_2$ complexes (**1a**, **1c**) are 20–30 ppm downfield compared to the $(PR_3)_2PdCl_2$ complexes (**2a**–**2c**, Table S4, Supporting Information) as observed in similar systems.[19] Ligand dissociation occurs upon dissolving the bisphosphine complexes (**2a**, **2b**) in $CDCl_3$ to give an equilibrium mixture of complex **2**, the $[(PR_3)Pd(\mu\text{-}Cl)Cl]_2$ complex (**1**), and free phosphine. In C_6D_6, less than 5% of ligand dissociation from **2a** to give free $P(t\text{-}Bu)_2Np$ and **1a** was observed. A larger extent (10%) of dissociation of $P(t\text{-}Bu)Np_2$ from **2b** was observed in C_6D_6. Ligand dissociation was not observed in the ^{31}P NMR spectrum of complex **2c** in either solvent. ^{31}P NMR chemical shifts were calculated for complexes **1a**–**1c** and **2a**–**2c**. The calculated chemical shifts were higher than the experimental values by 39.7–42.5 ppm for **1a**–**1c** and 16.6–22.4 ppm for **2a**–**2c**, similar to previously reported calculated ^{31}P NMR shifts.[20] Although the absolute shifts were too high, the calculated values accurately predicted the difference in chemical shift between the complexes within each series of compounds.

Structural analysis of $[(R_3P)Pd(\mu\text{-}Cl)Cl]_2$, *trans*-$(R_3P)_2PdCl_2$, and $(R_3P)_2Pd$ complexes. X-ray quality crystals of **1a**·$2CHCl_3$ were obtained by slow evaporation from chloroform (Figure 4). Diffusion of hexane into an acetonitrile solution of **1c** gave X-ray quality crystals of the solvent-free complex. Both structures were chloride-bridged dimers with coplanar palladium square planes. Alternate nonplanar polymorphic structures of **1a** and **1c** were obtained by diffusion of pentane into methylene chloride. The alternate structures had similar structural parameters apart from the angle between the palladium square planes (Figures S21 and S23, Tables S5 and S6, Supporting Information). Several single crystals of **1b** were obtained from various conditions, but all the crystals were disordered and gave low resolution structures.

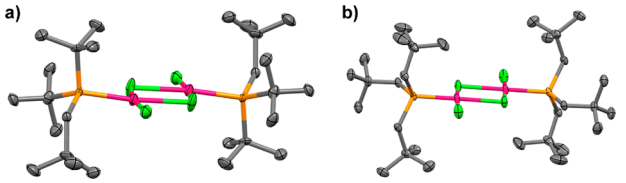

Figure 4. Thermal ellipsoid plots (50% probability) of $[(PR_3)Pd(\mu\text{-}Cl)Cl]_2$ complexes (**1a**, PR_3 = $P(t\text{-}Bu)_2Np$; **1c**, PR_3 = PNp_3). Hydrogen atoms and cocrystallized solvent (**1a**) are omitted for clarity. (a) **1a**, (b) **1c**. Structural data are provided in Table 1.

The crystal structure of **2a** has been previously reported by our group.[11c] Crystals of **2b** and **2c** were obtained by pentane diffusion into methylene chloride solutions. Like **2a**, complexes **2b** and **2c** crystallized with two molecules in the asymmetric unit with similar structural parameters (Figure 5 and Figures S24 and S25, Supporting Information). Both molecules in the asymmetric unit have a point of inversion at the palladium center. Data for the one molecules (Pd1) is discussed here, and values for both structures are reported in the Supporting Information (Tables S7–S9).

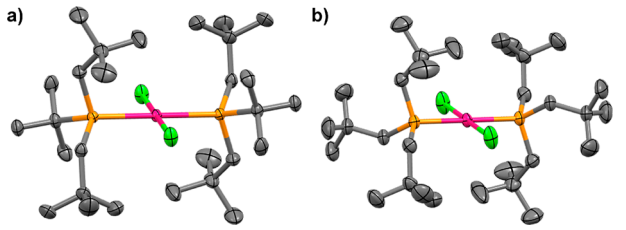

Figure 5. Thermal ellipsoid plots (50% probability) of $(R_3P)_2PdCl_2$ complexes (**2a**, PR_3 = $P(t\text{-}Bu)_2Np$; **2c**, PR_3 = PNp_3). Plots show one of two molecules in the asymmetric unit with hydrogen atoms omitted for clarity. (a) **2b**, (b) **2c**. Structural data are provided in Table 2.

Because complex **1b** did not give X-ray quality crystals, an alternative monophosphine complex of $P(t\text{-}Bu)Np_2$ was prepared to approximate the structure of **1b**. Structural characterization of $(PNp_3)Pd(Ar)(pyridine)Br$ complexes shows that pyridine ligands have little effect on the phosphine structure compared to halide-bridged analogs ($[(PNp_3)Pd(Ar)Br]_2$).[14] The reaction between **1b** and 4-picoline provided complete conversion to $[(P(t\text{-}Bu)Np_2)PdCl_2(4\text{-picoline})]$ (**3b**; eq 1). X-ray quality crystals of complex **3b** were obtained by cooling a concentrated solution of **1b** in methylene chloride with excess 4-picoline (Figure 6).

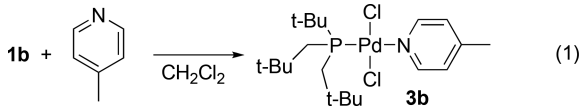

(1)

A comparison of selected experimental and calculated bond lengths and angles for complexes **1a**, **3b**, **1c**, and **2a**–**2c** are shown in Tables 1 and 2 (Figure 7). Crystal structures of Pd(0) complexes $(R_3P)_2Pd$ (PR_3 = $PtBu_2(Np)$ (**4a**),[11c] $PtBu(Np)_2$ (**4b**),[21] and $P(Np)_3$ (**4c**)[13a]) have been previously reported by our group (Figures S28–S30). Experimental and computational structural parameters are reported in Table S10

https://dx.doi.org/10.1021/acs.inorgchem.0c00266
Inorg. Chem. 2020, 59, 5579–5592

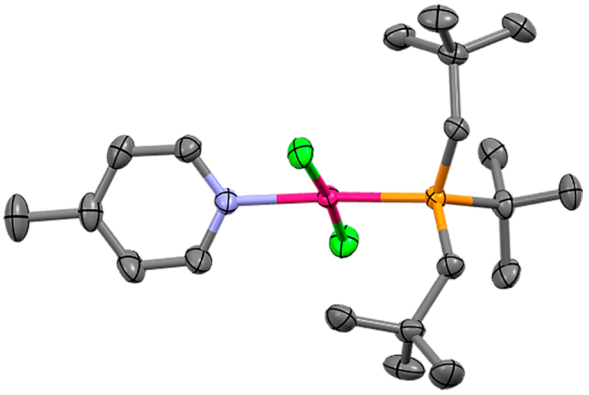

Figure 6. Thermal ellipsoid plot of $(P(t\text{-Bu})Np_2)PdCl_2$(4-picoline) (**3b**). Thermal ellipsoids drawn at the 50% probability level. Hydrogens are omitted for clarity.

(Supporting Information). The calculated structures were obtained at the DFT level using the BP86[22] and SVWN5[23] functionals. The DFT optimized structures with the BP86 and SVWN5 functionals bracket the experimental bond distances. The calculated bond angles are within 3° of experimental values. For **1a** and **3b**, the calculated and experimental torsion angles agree to experimental values within 5°. There is more variation between the computed and experimental torsion angles for **1c** with differences up to 20°.

The Pd−P bond lengths for the $(PR_3)PdCl_2(L)$ complexes (**1a** and **1c**, L = μ-Cl; **3b**, L = 4-picoline) are shorter than those in the $(PR_3)_2PdCl_2$ complexes **2a**−**2c**. The Pd−P bond distances also decrease as the number of neopentyl substituents increases (**1a** > **3b** > **1c**; **2a** > **2b** > **2c**), a trend consistent with decreasing front steric strain between the ligand and $PdCl_2$ unit.[6,7] The Pd−P distances in **2a** and **2b** are longer than that seen for $((P(t\text{-Bu})_3)P)_2Pd(H)Cl$ (2.361 Å),[24] whereas **2c** has a similar Pd−P bond length to the $P(t\text{-Bu})_3$ complex. The $L_2Pd(0)$ complexes (**4a**−**4c**) have shorter Pd−P bond lengths than **2a**−**2c**. The Pd−P bond lengths of **4a** and **4b** are similar to those of **1a** and **3b**, whereas PNp_3 complex **1c** has a shorter Pd−P bond length than **4c**. The Pd−P bonds of **4a**−**4c** are the same within error.

Monophosphine complexes **1a**, **3b**, and **1c** have slight seesaw distortions to the square plane with angles between trans ligands ranging from 168.25−179.20° (**1a**: τ_4 = 0.10, τ_4' = 0.07; **3b**: τ_4 = 0.09, τ_4' = 0.09; **1c**: τ_4 = 0.03, τ_4' = 0.02).[25] The angle between the phosphine and the cis μ-chloride is expanded (**1a** = 98.8°; **1c** = 95.6°) and the Cl−Pd−Cl angle for the bridging chlorides is compressed (**1a** = 83.2°; **1c** = 84.3°). In complex **3b**, the large P−Pd−Cl angle is for the chlorine that is nearly eclipsed with the *tert*-butyl substituent, and the chlorine that roughly bisects the Np−P−Np has a 90° P−Pd−Cl bond angle. The bis(phosphine) complexes (**2a**−**2c**) have nearly ideal square planar geometries with τ and τ' = 0 and cis L−Pd−L bond angles close to 90°.

The methylene unit of the neopentyl substituent provides a degree of flexibility through bond rotation (Pd−P−C−C dihedral angle), expansion of the P−C−C angle, and compression of the C−P−C angles. The response of the

Table 1. Selected Experimental and Computational Bond Lengths (Å) and Angles (deg) of Complexes 1a, 3b, and 1c

parameter[a]	**1a** expt[b]	**1a** calc BP86	**1a** calc SVWN	**3b** expt	**3b** calc BP86	**3b** calc SVWN	**1c** expt[b]	**1c** calc BP86	**1c** calc SVWN
Pd1−P	2.2869(6)	2.310	2.247	2.2758(9)	2.318	2.261	2.2362(6)	2.272	2.218
Pd1−Cl1′	2.3216(6)	2.370	2.309	2.3128(7)	2.343	2.310	2.3238(6)	2.382	2.327
Pd1−Cl2	2.2910(6)	2.323	2.273	2.3042(7)	2.362	2.288	2.2865(6)	2.317	2.267
Pd1−Cl1	2.4429(6)	2.465	2.391				2.4304(6)	2.467	2.392
P−C1	1.843(2)	1.879	1.835	1.857(2)	1.887	1.844	1.838(2)	1.871	1.831
P−C2	1.892(2)	1.941	1.887	1.859(3)	1.894	1.851	1.839(2)	1.876	1.835
P−C3	1.893(3)	1.933	1.883	1.885(3)	1.926	1.881	1.840(2)	1.869	1.833
P−Pd1−Cl1′	98.82(2)	99.1	97.8	89.68(3)	90.6	90.0	96.30(2)	96.3	95.8
P−Pd1−Cl2	91.79(2)	92.5	92.2	96.30(3)	95.3	93.8	87.46(2)	89.9	88.3
Cl2−Pd1−Cl1	86.19(2)	86.3	86.4	86.36(6)[c]	87.0[c]	87.9[c]	91.79(2)	90.0	90.8
Cl1′−Pd1−Cl1	83.16(2)	82.0	83.5	87.61(6)[c]	87.1[c]	88.3[c]	84.45(2)	83.7	85.0
Cl1′−Pd1−Cl2	168.25(2)	168.1	169.7	173.60(6)	173.8	173.9	176.22(3)	172.6	174.3
P−Pd1−Cl1	177.95(2)	177.5	177.0	173.99(3)[c]	177.6[c]	173.6[c]	179.20(3)	178.6	178.2
C1−P−C2	103.0(1)	102.3	102.8	107.2(1)	107.3	106.8	108.92(9)	107.9	107.1
C2−P−C3	107.9(1)	109.8	109.5	104.7(1)	104.2	104.5	101.80(9)	105.8	106.8
C3−P−C1	109.9(1)	108.6	108.1	98.1(1)	97.2	98.5	110.16(9)	106.7	107.3
$\sum_{C-P-C}$	320.8(2)	320.7	320.4	310.0(2)	308.7	309.8	320.9(2)	320.4	321.2
Pd1−P−C1	111.45(7)	112.6	112.5	112.36(8)	112.8	111.9	111.03(6)	114.0	113.6
Pd1−P−C2	116.71(8)	106.3	106.0	121.59(9)	121.0	121.5	113.10(6)	112.3	113.2
Pd1−P−C3	106.97(8)	116.4	116.9	110.13(9)	111.5	111.1	111.47(7)	109.7	108.5
$\sum_{Pd-P-C}$	335.1(1)	335.3	335.4	344.1(1)	345.3	344.5	335.6(1)	336.0	335.3
P−C1−C	126.9(1)	127.7	125.5	126.2(2)	126.9	124.3	125.7(1)	126.3	123.8
P−C2−C				125.5(2)	125.0	122.7	121.9(1)	123.6	121.2
P−C3−C							123.9(2)	123.3	120.5
Cl2−Pd1−P−C1	33.55(7))	32.4	32.1	33.11(9)	34.0	33.8	174.95(7)	164.3	165.5
Pd1−P−C1−C	61.4(2)	62.7	61.9	25.6(3)	25.1	26.0	170.9(1)	150.9	153.8
Pd1−P−C2−C				62.8(2)	62.8	61.7	41.9(2)	72.5	71.9
Pd1−P−C3−C							56.3(2)	47.6	46.8

[a]See Figure 7 for structure key. [b]Planar polymorph (Figure 4) was used for analysis. [c]Cl−Pd−N bond angle.

https://dx.doi.org/10.1021/acs.inorgchem.0c00266
Inorg. Chem. 2020, 59, 5579−5592

Table 2. Selected Experimental and Computational Bond Lengths (Å) and Angles (deg) of Complexes 2a−2c

parameter[a]	2a expt	2a calc BP86	2a calc SVWN	2b expt	2b calc BP86	2b calc SVWN	2c expt	2c calc BP86	2c calc SVWN
Pd1−P	2.4149	2.459	2.366	2.3893	2.437	2.353	2.3568	2.396	2.322
Pd1−Cl1	2.3035	2.351	2.300	2.3068	2.354	2.308	2.3055	2.359	2.309
P−C1	1.852(1)	1.887	1.843	1.854(2)	1.885	1.848	1.850(2)	1.880	1.838
P−C2	1.903(1)	1.941	1.890	1.854(2)	1.890	1.843	1.843(2)	1.876	1.840
P−C3	1.908(1)	1.946	1.893	1.900(2)	1.937	1.889	1.849(2)	1.877	1.838
P−Pd1−Cl1	90.80	91.3	90.9	91.85	92.0	91.1	91.85	90.9	91.9
P−Pd1−Cl1	89.20	88.7	89.1	88.15	88.0	88.9	88.15	89.1	88.1
Cl1−Pd1−Cl1	180.00	180.0	180.0	180.00	180.0	180.0	180.00	180.0	180.0
P−Pd1−P	180.00	180.0	180.0	180.00	180.0	180.0	180.00	180.0	180.0
C1−P−C2	100.92(6)	100.9	101.8	102.03(9)	100.7	101.8	107.18(9)	107.7	107.2
C2−P−C3	109.05(6)	108.7	108.5	99.74(9)	98.8	99.5	105.23(9)	104.0	105.4
C3−P−C1	106.87(6)	107.2	106.9	106.86(9)	107.4	107.0	105.78(9)	105.8	106.4
$\sum_{C-P-C}$	316.8(1)	316.8	317.2	308.6(2)	306.9	308.3	318.2(2)	317.5	319.0
Pd1−P−C1	112.59	113.0	112.6	115.26	114.2	113.7	111.71	111.7	112.3
Pd1−P−C2	105.53	105.2	104.7	120.16	120.4	120.7	117.05	117.6	117.5
Pd1−P−C3	120.14	119.9	120.5	110.25	112.6	111.7	109.15	109.3	107.2
$\sum_{Pd1-P-C}$	338.26	338.1	337.8	345.67	347.2	346.1	337.91	338.6	337.0
P−C1−C	126.2(1)	127.6	125.3	127.4(1)	127.1	125.2	127.9(1)	127.3	124.8
P−C2−C							123.4(1)	123.5	121.1
P−C3−C				126.5(2)	126.6	123.9	124.3(1)	123.6	120.7
Cl1−Pd1−P−C1	25.80	28.3	28.2	26.10	29.5	27.0	38.59	36.6	39.6
Pd1−P−C1−C	64.5	65.3	64.8	65.1	64.5	63.8	145.1	147.5	149.8
Pd1−P−C2−C							72.4	74.5	75.2
Pd1−P−C3−C				47.7	44.1	42.4	56.2	51.4	50.3

[a]See Figure 7 for structure key.

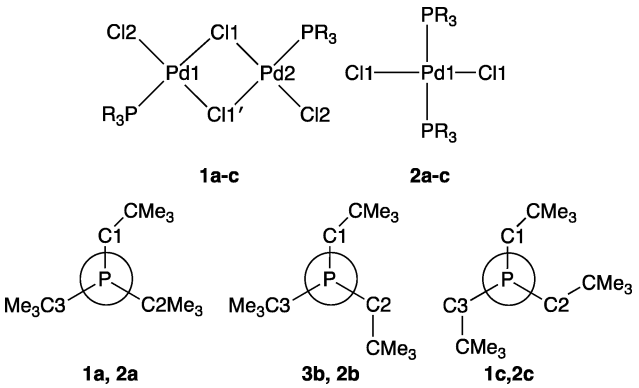

Figure 7. Key to structure descriptors used in Tables 2 and 3.

Pd−P−C−C dihedral angle can be seen most dramatically when comparing linear $L_2Pd(0)$ complexes (**4a**−**4c**, Table S10) and square planar palladium(II) complexes (**1a**, **3b**, **1c**, and **2a**−**2c**, Tables 1 and 2). The neopentyl group in the $Pd(P(t\text{-}Bu)_2Np)_2$ complex is eclipsed with the Pd−P bond (Pd1−P1−C1−C2 = 0.3(1)°). In the four coordinate complexes, the neopentyl substituent rotates away from the chloride ligand and adopts a gauche conformation to the Pd−P bond in the monophosphine complex (Pd1−P1−C1−C2 (**1a**) = 62.7(9)°) and the bisphosphine complex (Pd1−P1−C28−C30 (**2a**) = 64.5°).

A similar trend is seen with $P(t\text{-}Bu)Np_2$ and PNp_3 complexes. One of the neopentyl groups of $P(t\text{-}Bu)Np_2$ is eclipsed with the Pd−P bond in $Pd(P(t\text{-}Bu)Np_2)_2$ (Pd−P−C−C = 2.2(6)°) with the other neopentyl group also having a relatively small dihedral angle (29.6(6)°), whereas the dihedral angles are larger in **3b** and **2b**. The $Pd(PNp_3)_2$ complex has C_3 symmetry along the P−Pd−P axis with all the neopentyl substituents oriented toward the palladium with a Pd−C−C−C dihedral angle of 34.6°. The Pd(II) complexes of PNp_3 (**1c**, **2c**) adopt a conformation in which one neopentyl group is approximately anti to the Pd−P bond and the other two neopentyl groups are gauche (Pd−P−C−C: **1c** = 170.9(1)°, 56.3(2)°, 41.9(2)°; **2c** = 145.1°, 72.3°, and 56.2°). This pattern is consistent with other structurally characterized 4-coordinate complexes of trineopentylphosphine,[13a,14] as well as complexes of other primary alkylphosphines, such as PEt_3 and $P(n\text{-}Bu)_3$.[26]

Changing from linear to square planar structures results in an increase in the P−C−C angle of the neopentyl substituents. In $Pd(P(t\text{-}Bu)_2Np)_2$ (**4a**), the P−C−C angle of the neopentyl substituent is 119.62°. In the four-coordinate complexes (**1a**, **2a**), the neopentyl P−C−C angles increases to 126.7° (**1a**) and 126.2° (**1b**), respectively. A similar trend is seen with $P(t\text{-}Bu)Np_2$ and PNp_3. The two-coordinate L_2Pd complexes have neopentyl P−C−C angles similar to that of $Pd(P(t\text{-}Bu)_2Np)_2$. Palladium(II) $P(t\text{-}Bu)Np_2$ complexes **3b** and **2b** have neopentyl P−C−C angles ranging from 125.5 to 127.4° compared to 121° in **4b**. In the trineopentylphosphine system (**1c**, **2c**, and **4c**), the P−C−C angles of the neopentyl groups increase from 120.4° for the linear **4c** to 121.9−125.5° in $[(PNp_3)Pd(\mu\text{-}Cl)Cl]_2$ (**1c**) and 123.4−127.9° for $(PNp_3)_2PdCl_2$ (**2c**). The largest angle in each case is the neopentyl group *anti* to the Pd−P bond.

For each of the ligands, the $\sum_{C-P-C}$ value increases on going from the L_2Pd (**4**) to L_2PdCl_2 (**2**) to $[LPd(\mu\text{-}Cl)Cl]_2$ (**1**) complexes. Increased π-backbonding in the Pd(0) complexes compared to Pd(II) would be expected to result in smaller $\sum_{C-P-C}$ values.[27] Increased π-backbonding should also increase the P−C bond lengths. This trend is seen for the PNp_3 complexes (**4c** vs **1c**), but the $P(t\text{-}Bu)_2Np$ complexes

https://dx.doi.org/10.1021/acs.inorgchem.0c00266
Inorg. Chem. 2020, 59, 5579−5592

only show a statistically significant difference for the P−Np bond. The P(*t*-Bu)Np_2 P−C bond lengths do not have differences greater than 3σ.

Calculated $\sum_{C-P-C}$ values for the free ligands are similar to the values in the L_2Pd complexes (Table 3). The $\sum_{C-P-C}$ value for PNp_3 is similar to those of PEt_3 (299.4°) and PMe_3 (297.4°).[28] The pyramidalization of the neopentylphosphines does not change significantly upon complexing to palladium(0) (**4**). The free ligands all have smaller $\sum_{C-P-C}$ values than the palladium(II) complexes (**1a**, **1c**, **3b**, and **2a**−**2c**), which is expected with a less π-basic metal center.[6] The $\sum_{C-P-C}$ value for the low symmetry conformation of PNp_3 found in **1c** and **2c** was also calculated. This value is smaller than that of PNp_3 in **1c** and **2c**. The lower symmetry conformation of PNp_3 is higher in energy in the gas phase by 4.7 (SVWN5) and 5.7 (BP86) kcal/mol.

Table 3. Calculated $\sum_{C-P-C}$ Values for the Free Ligands

	$\sum_{C-P-C}$ (deg)		
functional	P(*t*-Bu)$_2$Np	P(*t*-Bu)Np_2	PNp_3
BP86	313.4	304.7	297.3[a]/311.0[b]
SVWN5	311.5	305.9	297.9[a]/309.2[b]

[a]Low energy C_3 symmetry configuration [b]Ligand in the optimized conformation found in complexes **1c** and **2c**

For the free ligands and the $L_2Pd(0)$ complexes, the phosphorus becomes increasingly pyramidalized as *tert*-butyl groups are replaced with neopentyl groups (PNp_3 < P(*t*-Bu)Np_2 < P(*t*-Bu)$_2$Np). In contrast, the trend with square planar palladium(II) centers is P(*t*-Bu)Np_2 < P(*t*-Bu)$_2$Np ≈ PNp_3. The $\sum_{C-P-C}$ value increases by approximately 7° for P(*t*-Bu)$_2$Np and P(*t*-Bu)Np_2 going from complex **4** to complex **1a** or **3b**. The increase is significantly larger for PNp_3 complexes **4c** and **1c** (25°), which accounts for the change in the trend. The larger change in $\sum_{C-P-C}$ value likely reflects the more significant conformational change that PNp_3 undergoes from the L_2Pd (**4c**) to the palladium(II) structures (**1c** and **2c**).

Ligand Steric Parameters. The steric properties of the neopentylphosphine ligands in different coordination environments were determined using the experimental and calculated structural data for the $(R_3P)_2Pd$, $[(R_3P)Pd(\mu\text{-Cl})Cl]_2$, and $(R_3P)_2PdCl_2$ complexes, as well as LPd^0 and $LPdCl_2$ (Table 4). In the case of the $L_2Pd(0)$ complexes (**4**), the solid cone angle increases as *tert*-butyl groups are replaced with neopentyl substituents (P(*t*-Bu)$_3$ < P(*t*-Bu)$_2$Np < P(*t*-Bu)Np_2 < PNp_3). The same trend is seen for calculated structures of LPd^0 complexes. The solid cone angles increase for P(*t*-Bu)$_2$Np and P(*t*-Bu)Np_2 in the palladium(II) complexes **1** and **2**. In contrast, the solid cone angle for PNp_3 decreases going from palladium(0) to palladium(II). As a result, the trend for the $(PR_3)PdCl_2L'$ (**1a**, **1c**, **3b**; P(*t*-Bu)$_2$Np ≈ PNp_3 < P(*t*-Bu)Np_2) and $(PR_3)_2PdCl_2$ (**2a**−**2c**; PNp_3 < P(*t*-Bu)$_2$Np < P(*t*-Bu)Np_2) indicate that PNp_3 is smaller than P(*t*-Bu)Np_2 and similar in size to P(*t*-Bu)$_2$Np in the square planar palladium(II) complexes. Cone angles for the calculated $LPdCl_2$ and L_2PdCl_2 follow the same trend of P(*t*-Bu)$_2$Np < P(*t*-Bu)Np_2

Table 4. Steric Parameters for P(*t*-Bu)$_3$, P(*t*-Bu)$_2$Np, P(*t*-Bu)Np_2, and PNp_3 Complexes

complex	Ω_{expt} (deg)[a]	Ω_{DFT} (deg)[a,b]	θ_{expt} (deg)[c]	θ_{DFT} (deg)[b,c]	$\%V_{bur(expt)}$ (%)[d]	$\%V_{bur\ (DFT)}$ (%)[b,d]	S4$_{expt}'$ (deg)[e]	S4$_{DFT}'$ (deg)[b,e]
				LPd^0				
(P(*t*-Bu)$_3$)Pd		191.0		191.0		38.1		6.9
(P(*t*-Bu)$_2$Np)Pd		208.5		194.5		41.7		22.7
(P(*t*-Bu)Np_2)Pd		216.2		206.4		44.5		40.2
(PNp3)Pd		217.8		200.7		45.5/40.0[f]		52.8/30.1
				L_2Pd^0				
(P(*t*-Bu)$_3$)$_2$Pd[g]	181.9	185.6	181.3	185.4	36.7	35.6	8.5	9.2
(P(*t*-Bu)$_2$Np)$_2$Pd (**4a**)	190.2	191.0	181.2	184.8	39.4	38.1	27.44	28.2
(P(*t*-Bu)Np_2)$_2$Pd (**4b**)	200.6	208.9	194.5	194.7	40.8	38.8	48.0	49.4
(PNp3)$_2$Pd (**4c**)	212.6	208.2	203.0	186.6	42.3	35.7	60.3	62.6
				$[LPd(\mu\text{-Cl})Cl]_2$				
$[(P(t\text{-Bu})_3)Pd(\mu\text{-Cl})Cl]_2$		192.1		180.5		34.2		7.0
$[(P(t\text{-Bu})_2Np)Pd(\mu\text{-Cl})Cl]_2$ (**1a**)	210.4	211.8	190.3	190.9	36.6	35.7	14.3	14.6
$[(P(t\text{-Bu})Np_2)Pd(\mu\text{-Cl})Cl]_2$ (**1b**)	218.4[h]	216.5	195.0[h]	197.5	38.4[h]	32.2/36.7[h]	34.1[h]	36.6
$[(PNp3)Pd(\mu\text{-Cl})Cl]_2$ (**1c**)	210.7	203.1	200.3	191.6	37.4	34.6	14.72	15.6
				$LPdCl_2$				
(P(*t*-Bu)$_3$)PdCl$_2$		198.6		187.1		36.6		1.2
(P(*t*-Bu)$_2$Np)PdCl$_2$		216.1		194.6		37.6		13.6
(P(*t*-Bu)Np_2)PdCl$_2$		219.8		200.9		38.1		26.4
(PNp3)PdCl$_2$		227.1		206.5		38.0		10.7
				L_2PdCl_2				
(P(*t*-Bu)$_3$)$_2$PdCl$_2$		185.8		170.8		29.2		14.8
(P(*t*-Bu)$_2$Np)$_2$PdCl$_2$ (**2a**)	205.1	203.2	180.9	182.9	33.2	32.1	21.42	21.3
(P(*t*-Bu)Np_2)$_2$PdCl$_2$ (**2b**)	210.3	204.3	185.7	187.5	33.9	32.4	37.04	40.0
(PNp3)$_2$PdCl$_2$ (**2c**)	203.4	215.5	183.9	184.3	32.4	32.3	19.72	21.1

[a]Solid cone angle determined using the STERIC program.[4b] [b]BP86/DZVP2 optimized geometries. [c]Exact cone angle determined by the Allen method[3] [d]Percent buried volume calculated with SambVca 2.0[5c] [e]S4′ = $\sum_{Pd-P-C} - \sum_{P-C-C}$. [f]The first value is for the optimal C_3 symmetry configuration found in the free ligand, and the second value is for the ligand in the optimized conformation found in the palladium complex. [g]Experimental values determined from reported crystal structure.[29] [h]Determined from crystal structure of **3b**

https://dx.doi.org/10.1021/acs.inorgchem.0c00266
Inorg. Chem. 2020, 59, 5579−5592

< PNp_3. Exact cone angles (θ) were calculated using Allen's method.[3] The exact cone angles were smaller than the solid cone angles by 0−20° but followed similar trends.

The $\%V_{bur}$ for the ligands depends on the coordination environment at palladium (Table 4). In the two-coordinate L_2Pd^0 complexes, the $\%V_{bur}$ values increase as additional neopentyl groups are added ($P(t\text{-Bu})_3$ < $P(t\text{-Bu})_2Np$ < $P(t\text{-Bu})Np_2$ < PNp_3). The LPd complexes follow the same trend with larger values. The 4-coordinate $[LPd(\mu\text{-Cl})Cl]_2$ complexes have smaller $\%V_{bur}$ values than the L_2Pd^0 complexes. The decrease in $\%V_{bur}$ is largest for PNp_3 and smallest for $P(t\text{-Bu})Np_2$. As a result, the $\%V_{bur}$ increases in the order $P(t\text{-Bu})_2Np$ < PNp_3 < $P(t\text{-Bu})Np_2$. Adding a second phosphine to the coordination sphere further decreases the $\%V_{bur}$ for all three ligands, with PNp_3 having the largest decrease. The ordering for the L_2PdCl_2 complexes is PNp_3 < $P(t\text{-Bu})_2Np$ < $P(t\text{-Bu})Np_2$.

Experimental and calculated structures for the neopentylphosphine series give similar S4′ values (Table 4). For the LPd and L_2Pd complexes, the S4′ parameter increases in the order $P(t\text{-Bu})_3$ < $P(t\text{-Bu})_2Np$ < $P(t\text{-Bu})Np_2$ < PNp_3. Previously reported values of S4′ for $P(t\text{-Bu})_3$ (7.4), $P(t\text{-Bu})_2Np$ (23.3°), $P(t\text{-Bu})Np_2$ (43.4°), and PNp_3 (48.6°) based on calculated LAuCl structures are similar to those calculated for LPd complexes.[10b] Significantly, the S4′ parameter for these ligands correlates positively with cone angle and $\%V_{bur}$ values, which is opposite of the expected trend.[7]

The palladium(II) complexes have smaller S4′ values than the palladium(0) complexes due in part to decreased π backbonding from palladium. The L_2PdCl_2 complexes have larger S4′ values for each ligand than the $[LPd(\mu\text{-Cl})Cl]_2$ complexes. For all of the palladium(II) complexes analyzed, $P(t\text{-Bu})_2Np$ and PNp_3 have similar S4′ values, whereas $P(t\text{-Bu})Np_2$ has a significantly larger value. For example, in the L_2PdCl_2 complexes, the values are PNp_3 = 19.72°, $P(t\text{-Bu})_2Np$ = 21.42°, and $P(t\text{-Bu})Np_2$ = 37.04°. These values correlate positively with cone angle and $\%V_{bur}$ values, rather than the expected inverse correlation.

Analysis of Ligand Electronic Properties. The proton affinity (PA) is a measure of the Lewis basicity of the phosphines. The proton affinities of the phosphines were calculated at the BP86 and SVWN5 levels (Table 5). The PA was benchmarked by calculating the values for PH_3 and PMe_3 at the DFT levels as well as at the G3MP2 level.[30] There is good agreement between the G3MP2 values and experimental values,[31] and the BP86 values are also in agreement with the experimental and the G3MP2 calculated values within 2 kcal/mol. The PA for the low symmetry PNp_3 conformation found in complexes **1c** and **2c** is higher than in the optimal C_3 structure. The PA values have little variation between the ligands but increase in the order $PNp_3 \lesssim P(t\text{-Bu})Np_2$ < $P(t\text{-Bu})_2Np$. The trend is similar to that previously reported by us with other electronic descriptors, including CO stretching frequencies of *trans*-$(R_3P)_2Rh(CO)Cl$ complexes, calculated charge on phosphorus of the free ligands, and HOMO energy levels for the free ligand.[11b]

Table 5. Phosphines Proton Affinities at 298 K in kcal/mol for Different DFT Starting Geometries

phosphine	BP86	SVWN5	G3MP2	exp
$P(t\text{-Bu})_2Np$	240.9	233.3		
$P(t\text{-Bu})Np_2$	237.6	230.4		
PNp_3	236.4/240.2[a]	230.0/232.4[a]		
PH_3	185.7	178.9	187.3	187.3[31]
PMe_3	226.4	219.9	228.1	229.2[31]

[a]Using the experimental conformation in **2c**

Ligand Binding Equilibria. Complexes **2a** and **2b** undergo ligand dissociation in solution to establish an equilibrium between the corresponding monophosphine dimer (**1a−1c**), free phosphine, and the diphosphine complex (**2a−2c**). Quantification of the equilibrium constants for these reactions would provide a way to assess the effective steric demand of these ligands as it affects ligand binding equilibria. Reaction equilibria were measured by analyzing the bridge cleavage reaction of complexes **1a−1c** with neopentylphosphines (eq 2, Table 6). Solutions with varied concentrations of

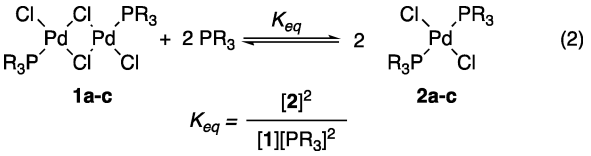

(2)

the palladium dimer complex (**1**) and free ligand were analyzed by ^{31}P NMR spectroscopy in both C_6D_6 and $CDCl_3$. The reactions reached equilibrium within minutes and showed no further change over time.

Phosphine binding to **1a−1c** was exothermic for all three ligands, resulting in equilibrium constants ranging from 10^2 to 10^6. For all three complexes, the equilibrium constants obtained in C_6D_6 were larger than those measured in $CDCl_3$. For $P(t\text{-Bu})_2Np$ and $Pt\text{-Bu}(Np)_2$, the equilibrium constant was an order of magnitude larger in benzene compared to chloroform, whereas the difference was only a factor of 2 for PNp_3. For each solvent system, the equilibrium constants increased in the order $Pt\text{-Bu}(Np)_2$ < $P(t\text{-Bu})_2Np$ < PNp_3, with the difference between each ligand being 1−2 orders of magnitude. The binding equilibria correlate positively with the cone angle, $\%V_{bur}$, and S4′ trends for complexes **1** and **2**.

The binding equilibria were also analyzed computationally. The binding of phosphine to $[(PR_3)Pd(\mu\text{-Cl})Cl]_2$ complexes **1a−1c** (eq 2) can be considered to occur in two different steps: (1) dissociation of $[(PR_3)Pd(\mu\text{-Cl})Cl]_2$ into two molecules of $(PR_3)PdCl_2$ (Reaction 3) and (2) addition of the phosphine to $(PR_3)PdCl_2$ (Reaction 4). The energy of reaction 2 is then 3 + 2(4).

$$[(PR_3)Pd(\mu\text{-Cl})Cl]_2 \rightarrow 2(PR_3)PdCl_2 \quad (3)$$

$$(PR_3)PdCl_2 + PR_3 \rightarrow (PR_3)_2PdCl_2 \quad (4)$$

To benchmark the DFT functionals, the energy of reaction 3 with PR_3 = PH_3 was calculated at the Feller−Peterson−Dixon (FPD) level[32] using coupled cluster CCSD(T) theory calculations extrapolated to the complete basis set limit plus additional corrections (Tables S11). The energy for reaction 4 at the FPD level was previously reported.[33] The correction factors determined from the FPD calculations on $[(PH_3)Pd(\mu\text{-Cl})Cl]_2$ were used for the larger phosphines, an approximation that does not consider additional corrections for steric effects. Single point energies were calculated with a variety of gradient corrected functionals which treat long-range steric interactions in different ways: BP86,[22] B3LYP,[34] ωB97x-D,[35] CAM-B3LYP,[36] M06,[37] TPSS,[38] and HSEh1PBE.[39]

https://dx.doi.org/10.1021/acs.inorgchem.0c00266
Inorg. Chem. 2020, 59, 5579−5592

Table 6. Equilibrium Constants from the Measured Equilibrium Concentrations and Experimental and Calculated Free Energies (298 K in kcal/mol) for the Reaction of $[(R_3P)Pd(\mu\text{-}Cl)Cl]_2$ and $2PR_3$ to Give $2(R_3P)_2PdCl_2$ (eq 2)

ligand	solvent	K_{eq} $(M^{-1})^a$	$\Delta G_{expt}{}^b$	BP86	B3LYP	ωB97x-D	M06	CAM-B3LYP	HSEh1PBE	TPSS
H_3P	C_6D_6			−18.8	−18.8	−18.7	−18.5	−18.8	−18.5	−18.7
$P(t\text{-}Bu)_3$	C_6D_6			21.2	23.0	4.6	3.9	20.8	18.3	20.3
$P(t\text{-}Bu)_2Np$	C_6D_6	$(2.4 \pm 0.2) \times 10^5$	-7.32 ± 0.06	5.7	7.2	−19.7	−16.4	2.7	0.7	4.7
$P(t\text{-}Bu)Np_2$	C_6D_6	$(6.4 \pm 0.4) \times 10^3$	-5.18 ± 0.04	8.2	9.2	−17.8	−14.6	4.4	3.0	7.2
PNp_3	C_6D_6	$(1.98 \pm 0.08) \times 10^6$	-8.58 ± 0.03	−4.7	−3.2	−33.2	−26.7	−7.5	−8.8	−4.5
H_3P	$CDCl_3$			−20.0	−20.2	−20.0	−20.0	−20.2	−20.0	−20.0
$P(t\text{-}Bu)_3$	$CDCl_3$			24.6	26.2	7.8	7.1	24.0	21.7	23.5
$P(t\text{-}Bu)_2Np$	$CDCl_3$	$(1.4 \pm 0.2) \times 10^4$	-5.63 ± 0.07	8.7	10.2	−16.5	−13.4	5.7	3.9	7.7
$P(t\text{-}Bu)Np_2$	$CDCl_3$	$(7.4 \pm 0.2) \times 10^2$	-3.91 ± 0.02	11.2	12.0	−15.0	−11.6	7.2	6.1	10.1
PNp_3	$CDCl_3$	$(9.1 \pm 0.5) \times 10^5$	-8.12 ± 0.03	−2.9	−1.4	−31.4	−24.9	−5.7	−7.0	−2.7

[a]Value determined experimentally by ^{31}P NMR analysis of the cleavage of dimer **1** with phosphine. [b]Calculated from experimentally determined K_{eq} value

All the functionals predict reaction 3 to be endothermic with the B3LYP and BP86 functionals predicting the least endothermicity (Table S12, SI). The endothermicities for all the functionals fall in the range of 8.5 to 14.0 kcal/mol for the neopentylphosphines. The reactions are predicted to be less endothermic in $CHCl_3$ than in C_6H_6. The smallest endothermicities are predicted for $P(t\text{-}Bu)_3$, suggesting that it has the largest steric effect. The dimer dissociation energy is predicted to be within 1 kcal/mol for each neopentylphosphine using all the functionals, except M06 and ωB97x-D.

For reaction 4, there is a wider range of ligand bond energies depending on the functional (Table S13, Supporting Information). This value has a factor of 2 impact on the energy of reaction 2, so it contributes significantly to the overall energy. The BP86, B3LYP, CAMB3LYP, HSEh1PBE, and TPSS functionals all show binding energies between 0 and −10 kcal/mol in C_6H_6 indicating exothermic binding. In $CHCl_3$, these five functionals show that PNp_3 binds exothermically but that $P(t\text{-}Bu)_2Np$ and $P(t\text{-}Bu)Np_2$ have endothermic or slightly exothermic binding (+2.1 to −2.3 kcal/mol). The ωB97x-D and M06 functionals lead to significantly larger binding energies of −14 to −22 kcal/mol. Thus, the latter two functionals predict smaller steric interactions between the two ligands on $(PR_3)_2PdCl_2$ than the first five functionals. In all cases, the binding energy of the second ligand is in the order of $PNp_3 > P(t\text{-}Bu)_2Np > P(t\text{-}Bu)Np_2 \gg P(t\text{-}Bu)_3$. $P(t\text{-}Bu)_3$ is not predicted to bind to $(P(t\text{-}Bu)_3)PdCl_2$ except for very weak binding in C_6H_6 with the ωB97x-D and M06 functionals.

The calculated values for reaction 2 in Table 6 show that each functional predicts the correct order for the reactivity for the ligands in comparison to the experiment ($PNp_3 > P(t\text{-}Bu)_2Np > P(t\text{-}Bu)Np_2 > PNp_3$). All the functionals predict that the energies for reaction 2 are less exothermic or more endothermic in $CHCl_3$ than in C_6H_6. For reaction 2 energies, the HSEh1PBE functional gave excellent agreement for PNp_3, but the energies for $P(t\text{-}Bu)_2Np$ and $Pt\text{-}Bu(Np)_2$ were too endothermic.

Modest errors of a few kilocalories per mole in each reaction step can significantly affect the calculated energies for reaction 2. The calculations with the BP86, B3LYP, CAMB3LYP, HSEh1PBE, and TPSS functionals likely overestimate the binding energy of $[(PR_3)Pd(\mu\text{-}Cl)Cl]_2$ (**1**) and underestimate the binding energy of the second phosphine in $(PR_3)_2PdCl_2$ (**2**). In contrast, the ωB97x-D and M06 functionals predict that the dimer is strongly bound and the binding energy of the second phosphine in $(PR_3)_2PdCl_2$ is too large. The large binding energy in reaction 4 dominates and makes the energy of reaction 2 too negative.

DISCUSSION

Our group has previously hypothesized about the impact of the conformational flexibility of neopentylphosphines, particularly trineopentylphosphine, on catalytic performance.[11d,f,12−14] The structural analysis of these ligands reported here provides quantitative data on the impact of these structural changes on the steric properties of these ligands in different coordination environments. Due to the more significant conformational change for PNp_3 compared to $P(t\text{-}Bu)_2Np$ and $P(t\text{-}Bu)Np_2$, the relative ordering in steric demand changes depending on the coordination number of the metal complex. For the linear palladium(0) complexes, solid cone angle, exact cone angle, and $\%V_{bur}$ all show that the steric trend is $P(t\text{-}Bu)_3 < P(t\text{-}Bu)_2Np < P(t\text{-}Bu)Np_2 < PNp_3$. This trend is consistent with calculated steric trends based on the He_8 steric parameter for these ligands.[10] In square planar palladium(II) complexes, the ordering for these steric descriptors is $P(t\text{-}Bu)_3 < PNp_3 \lesssim P(t\text{-}Bu)_2Np < P(t\text{-}Bu)Np_2$. Thus, PNp_3 is predicted to have the largest steric demand in linear palladium(0) complexes and the smallest in square planar palladium(II) complexes for the neopentylphosphine series.

Both the solid cone angle and exact cone angle give increasing values going from linear L_2Pd (**1**) to square planar L_2PdCl_2 (**2**) to $[LPd(\mu\text{-}Cl)Cl]_2$ (**1**) complexes with the exception of PNp_3 as noted previously. This trend is unexpected as cone angles have been shown to decrease as the coordination number increases.[40] Although the neopentyl group does rotate away from the metal center, the ligand retains a significant steric impact and results in increased steric interaction between the palladium and the *tert*-butyl group(s). For example, in $Pd(P(t\text{-}Bu)_2Np)_2$ (**4a**), the closest Pd−C distance for the neopentyl group is 3.604 Å and the closest *tert*-butyl Pd−C distance is 3.727 Å. In **2a**, the neopentyl distance increases to 3.701 Å as the Pd−P−C-C dihedral increases, but the Pd−P−C angle to one of the *tert*-butyl groups decreases, resulting in the nearest *tert*-butyl carbon being closer to palladium (3.545 Å). Overall, these changes result in an increase in cone angle. In the case of **1a**, the neopentyl (3.599 Å) and *tert*-butyl groups have closer contacts (3.360 Å) than in either **2a** or **4a**, likely due to the shorter Pd−P bond in **1a**.

Although the neopentylphosphines have larger cone angle and buried volume values than $P(t\text{-}Bu)_3$ based on our

https://dx.doi.org/10.1021/acs.inorgchem.0c00266
Inorg. Chem. 2020, 59, 5579−5592

structural analysis (Table 4), it is not clear that they are in fact more sterically demanding. Within the neopentyl series, the binding equilibria (Table 6) follow the trend in steric demand for the palladium(II) complexes. The low stability of the $[(P(t\text{-}Bu)_3)Pd(\mu\text{-}Cl)Cl]_2$ and $(P(t\text{-}Bu)_3)_2PdCl_2$ complexes did not allow us to compare the binding equilibria of $P(t\text{-}Bu)_3$ with the neopentylphosphines. Calculated ΔG values for this system show that $P(t\text{-}Bu)_3$ binding is much more endothermic than the neopentylphosphines, suggesting that it is effectively larger. $P(t\text{-}Bu)_3$ is also able to enforce a three-coordinate T-shaped structure in $(P(t\text{-}Bu)_3Pd(Ar)X$ complexes,[41] whereas $P(t\text{-}Bu)_2Np$ and PNp_3 give halide-bridged dimers.[11f,13,14] In contrast, Pd−P bond lengths for $(PR_3)_2PdCl_2$ complexes **2a**−**2c** are the same as (**2c**) or longer than for $(P(t\text{-}Bu)_2Pd(H)Cl$, suggesting a similar or larger steric effect for the neopentylphosphines. The steric bulk of $P(t\text{-}Bu)_3$ is closer to the phosphorus and more rigid than in the case of PNp_3. Although PNp_3 may have a larger cone angle and buried volume, this steric demand is more distant from the metal and appears to have a less significant steric impact on the metal, at least in some cases, than does $P(t\text{-}Bu)_3$.

The degree of pyramidalization at a phosphorus center is sensitive to both steric and electronic effects. Pyramidalization at phosphorus lowers the energy of the HOMO orbital, which is primarily the phosphorus lone pair.[27a] In the absence of steric strain, highly pyramidalized structures are favored, such as PH_3 ($\sum_{H-P-H}$= 279°). As the substituents on phosphorus become larger, steric repulsion requires that the Z−P−Z angles increase, resulting in a more planar structure. Upon complexation to a metal, σ donation from phosphorus depopulates the phosphorus HOMO, resulting in a decreased pyramidalization.[6] This effect is offset by π-backbonding from the metal, which increases pyramidalization.

Across a wide range of phosphines and metal complexes, S4′, which is a measure of pyramidalization, has been found to correlate negatively with cone angle and $\%V_{bur}$, since larger substituents typically result in a more planar phosphorus.[6,7,40] In the neopentylphosphine series, S4′ has a strong positive correlation with increasing cone angle and $\%V_{bur}$. The key to this behavior appears to be the that the sterically demanding substituent is separated from the phosphorus by a methylene spacer. The neopentyl group can exert a large steric demand, while accommodating a more pyramidalized phosphorus. As a result, pyramidalization as measured by S4′ and steric parameters have a direct, rather than inverse, relationship.

In free trineopentylphosphine, the phosphorus is highly pyramidalized because of the relatively small back-side strain of the methylene units (Figure 8). The bulky CMe_3 unit is projected toward the front side of the phosphorus center, where they can exert a large steric demand. When the neopentyl groups are replaced with *tert*-butyl substituents ($P(t\text{-}Bu)Np_2$ and $P(t\text{-}Bu)_2NP$), the larger back strain of the *t*-Bu group forces the phosphorus to become more planar. Complexation to palladium(0) to give L_2Pd complexes (**4**) results in little change in the phosphine conformation or the degree of pyramidalization. The effects of the σ donation from phosphorus and π backbonding from the metal appear to largely cancel out.

Coordination of PNp_3 to a square planar palladium(II) center results in a significant conformation change that rotates one neopentyl group anti to the P−Pd bond. This results in a significant decrease in the pyramidalization of phosphorus as the back-side strain is increased (Figure 8). The steric demand

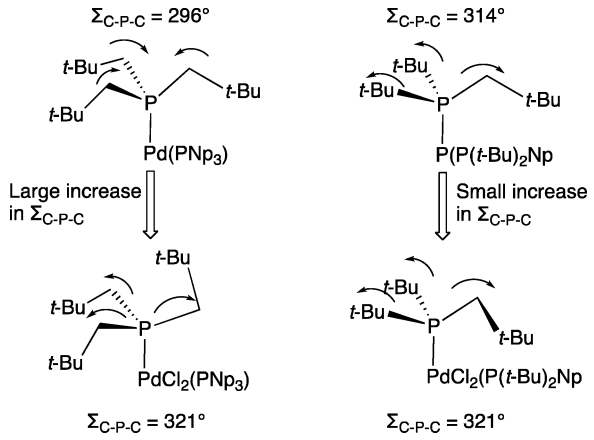

Figure 8. Changes in degree of pyramidalization in neopentylphosphines.

of PNp_3 is also decreased as a result. $P(t\text{-}Bu)_2Np$ and $P(t\text{-}Bu)Np_2$ undergo less significant conformational changes upon coordination to a palladium(II) center, resulting in smaller decreases in the degree of pyramidalization and changes in steric demand. As a result, PNp_3 has larger steric parameters and is more pyramidal than $P(t\text{-}Bu)_2Np$ and $P(t\text{-}Bu)Np_2$ as a free ligand and when complexed to palladium(0). When complexed to a palladium(II) center, PNp_3 has similar steric demand and pyramidalization to $P(t\text{-}Bu)_2Np$ and is smaller and less pyramidal than $P(t\text{-}Bu)Np_2$. The two neopentyl substituents of $P(t\text{-}Bu)Np_2$ are in gauche relationships to the Pd−P bond. As a result there is less back strain than in $P(t\text{-}Bu)_2Np$ or PNp_3, allowing the phosphorus to be more pyramidal. The neopentyl groups of $P(t\text{-}Bu)Np_2$ still exert significant steric demand on the coordinated metal.

Palladium-catalyzed cross-coupling reactions involve both linear palladium(0) species (L_2Pd and LPd) and square planar or T-shaped palladium(II) complexes. In the oxidative addition step, more sterically demanding ligands, that favor the LPd species, provide more active catalysts. On the basis of this trend, PNp_3, which is more sterically demanding than $P(t\text{-}Bu)_2Np$ when complexed to Pd(0), might be expected to give a more active catalyst than $P(t\text{-}Bu)_2Np$. In fact, the opposite is true in a variety of cross-coupling reactions.[11a,b] One interpretation of this result would be that ligand dissociation from $(PNp_3)_2Pd$ is less favorable than the analogous $P(t\text{-}Bu)_3$ or $P(t\text{-}Bu)_2Np$ as is seen for the palladium(II) complexes. The more distant steric bulk of the neopentyl group may be less effective at promoting the low coordination LPd species, compared to *t*-Bu-substituted phosphines. The Pd−P bond lengths of the $(PR_3)_2Pd$ complexes (**4a**−**4c**) suggest that there is little difference in the front side strain in these complexes. Alternatively, this trend may indicate that ligand steric effects on the palladium(II) species on the catalytic cycle are more important for the catalyst performance.

The $PNpP_3$ ligand provides more effective catalysts for cross-coupling of sterically demanding aryl bromides.[11e,13] The effectiveness of these catalyst systems appears to correlate with the steric demand in the palladium(II) complexes on the catalytic cycle. This result may suggest that the stability of the resulting oxidative addition products is a more important factor in catalyst productivity than the rate of oxidative addition. We have observed that $[(PNp_3)Pd(Ar)X]_2$ complexes are more stable than $[(P(t\text{-}Bu)_2Np)Pd(Ar)X]_2$ complexes, which are more prone to arene elimination to afford catalytically inactive

https://dx.doi.org/10.1021/acs.inorgchem.0c00266
Inorg. Chem. 2020, 59, 5579−5592

palladacyclic species.[11f,13b] Alternatively, the $(PNp_3)Pd$ complex may be more reactive with sterically hindered aryl halides than $(P(t\text{-}Bu)_2Np)Pd$, despite its larger cone angle, because the steric bulk is further from the metal and more flexible.

CONCLUSIONS

Analysis of the series of $P(t\text{-}Bu)_nNp_{3-n}$ ($n = 0-3$) has provided a detailed picture of the structure and steric demand of these ligands. The structures of the free ligands and their linear palladium(0) complexes show a consistent trend of increasing steric demand and increasing pyramidalization as the number of neopentyl groups is increased ($P(t\text{-}Bu)_3 < P(t\text{-}Bu)_2Np < P(t\text{-}Bu)_2Np < PNp_3$). In square planar palladium(II) complexes, the trend is $P(t\text{-}Bu)_3 < PNp_3 < P(t\text{-}Bu)_2Np < P(t\text{-}Bu)_2Np$. This change in order is due to the dramatic conformational change that PNp_3 undergoes upon coordination to a square planar metal center, which results in a smaller cone angle and decreased pyramidalization of the phosphorus. The other neopentyl ligands do not undergo a similar conformational change.

This study shows that care must be taken when using steric parameters, particularly for ligands with a high degree of conformational flexibility and those in which the steric demand is more remote from the metal center. Steric parameters determined for low-coordinate metal complexes, such as the commonly used LAuCl, may overestimate steric demand for higher coordination number complexes that may be relevant to catalytic systems. More importantly, the relative ordering of ligands may be inaccurate. Last, care must be taken when considering steric parameters of ligands in which the steric bulk has different radial distributions relative to the metal. Although larger steric parameter values are obtained for neopentylphosphines than $P(t\text{-}Bu)_3$, there is evidence to suggest that $P(t\text{-}Bu)_3$ has a larger effective steric demand on a metal center. This may be due to the fact that the steric demand of a *tert*-butyl group is located closer to the metal center and is more rigid than the neopentyl groups of PNp_3.

EXPERIMENTAL SECTION

General Methods. $P(t\text{-}Bu)_2Np$,[42] $P(t\text{-}Bu)Np_2$,[42] PNp_3,[42] and $[(P(t\text{-}Bu)_2Np)Pd(\mu\text{-}Cl)Cl]_2$[11f] were prepared according to literature procedures. $(CH_3CN)_2PdCl_2$ was prepared by refluxing palladium dichloride in acetonitrile and was freshly prepared as needed. Toluene was dried and deoxygenated by refluxing over sodium and distilling under nitrogen. Methylene chloride was distilled over CaH_2 and deoxygenated under a vacuum. C_6D_6 and $CDCl_3$ were deoxygenated under a vacuum. All other solvents and reagents were used as received.

General Method for the Synthesis of $[(R_3P)Pd(\mu\text{-}Cl)Cl]_2$. In a glovebox, $(CH_3CN)_2PdCl_2$ (1 equiv) and R_3P (0.8 equiv) were added to an oven-dried flask. The flask was sealed and removed from the drybox. Anhydrous toluene (2 mL) and anhydrous methylene chloride (1 mL) were added to the reaction flask via syringe under N_2 flow. The reaction was stirred under N_2(g) at ambient temperature overnight. The crude reaction mixture was exposed to air and filtered over a plug of Celite to remove any undissolved solids. The solvent was removed under reduced pressure to yield the product as a solid. In some cases, the product was further purified via recrystallization from hot hexanes.

$[(P(t\text{-}Bu)Np_2)Pd(\mu\text{-}Cl)Cl]_2$ (1b). $(CH_3CN)_2PdCl_2$ (50 mg, 0.2 mmol) and $P(t\text{-}Bu)Np_2$ (37 mg, 0.16 mmol) were reacted following the general method. Product was purified via recrystallization from hexanes to yield 40 mg (61%) of the product as a red-orange crystalline solid. ^1H NMR (500 MHz, $CDCl_3$): δ 2.22 (dd, J = 13.0, 15.0 Hz, 4H), 1.84 (dd, J = 13.0, 15.0 Hz, 4H) 1.44 (d, J_{P-H} = 15.6 Hz, 18H), 1.44 (s, 36H). ^{13}C NMR (125 MHz, $CDCl_3$): δ 40.5 (d, J_{P-C} = 21.2 Hz), 35.6 (d, J_{P-C} = 23.4 Hz), 33.5 (d, J_{P-C} = 6.7 Hz), 31.7 (d, J_{P-C} = 4.2 Hz), 29.0 (d, J_{P-C} = 2.7 Hz). $^{31}P\{^1H\}$ NMR (MHz, $CDCl_3$): δ 49.59 (s). Anal. Calcd for $C_{28}H_{62}Cl_4P_2Pd_2$: C, 41.24; H, 7.26; Cl, 17.39. Found: C, 41.07; H, 7.56; Cl, 17.51.

$[(PNp_3)Pd(\mu\text{-}Cl)Cl]_2$ (1c).[43] $(CH_3CN)_2PdCl_2$ (100 mg, 0.4 mmol) and PNp_3 (76 mg, 0.3 mmol) were reacted following the general method to yield 121 mg (93%) of the product as an orange solid. ^1H NMR (500 MHz, C_6D_6): δ 1.68 (d, J_{P-H} = 13.2 Hz, 12H), 0.95 (s, 54H). ^{13}C NMR (125 MHz, $CDCl_3$): δ 38.7 (d, J_{P-C} = 24.9 Hz), 33.2 (d, J_{P-C} = 6.7 Hz), 32.7 (d, J_{P-C} = 5.1 Hz). $^{31}P\{^1H\}$ NMR (MHz, $CDCl_3$): δ 26.54 (s). Anal. Calcd for $C_{30}H_{66}Cl_4P_2Pd_2$: C, 42.72; H, 7.89; Cl, 16.81. Found: C, 43.00; H, 8.04; Cl, 17.09.

General Method for the Synthesis of $(R_3P)_2PdCl_2$. In a glovebox, $(CH_3CN)_2PdCl_2$ (1 equiv) and R_3P (2 equiv) were added to an oven-dried flask. The flask was sealed and removed from the drybox. Anhydrous toluene (2−3 mL) was added to the reaction flask via syringe under N_2 flow. The reaction was stirred under N_2 at ambient temperature overnight. The crude reaction mixture was exposed to air and filtered over Celite to remove any undissolved solids. The solvent was removed under reduced pressure to yield the product as a solid. In some cases, the product was further purified via recrystallization from hot hexanes.

$(P(t\text{-}Bu)_2Np)_2PdCl_2$ (2a).[11c] $(CH_3CN)_2PdCl_2$ (50 mg, 0.2 mmol) and $P(t\text{-}Bu)_2Np$ (103 μL, 0.4 mmol) were reacted following the general method to yield 100.1 mg (82%) of the product as a yellow solid. ^1H NMR (500 MHz, C_6D_6): δ 1.96 (m, 4H), 1.29 (vt, J_{P-H} = 6.4 Hz, 36H), 1.17 (s, 18H). ^{13}C NMR (125 MHz, C_6D_6): δ 37.1 (t, J_{P-C} = 6.7 Hz), 33.5 (br), 31.3, 31.1, 30.4 (t, J_{P-C} = 4.5 Hz). $^{31}P\{^1H\}$ NMR (MHz, C_6D_6): δ 43.6. Anal. Calcd for $C_{26}H_{58}Cl_2P_2Pd$: C, 51.19; H, 9.58; Cl, 11.62. Found: C, 50.73; H, 9.50; Cl, 11.89.

$(P(t\text{-}Bu)Np_2)_2PdCl_2$ (2b). $(CH_3CN)_2PdCl_2$ (50 mg, 0.2 mmol) and $P(t\text{-}Bu)Np_2$ (92 mg, 0.4 mmol) were reacted following the general method. The crude mixture was purified via recrystallization from hexanes to yield 73 mg (57%) of the product as a yellow crystalline solid. ^1H NMR (500 MHz, C_6D_6): δ 2.35 (m, 4H), 1.88 (m, 4H), 1.43 (m, 54H). ^{13}C NMR (125 MHz, C_6D_6): δ 38.8 (t, J_{P-C} = 7.0 Hz), 34.3 (t, J_{P-C} = 9.8 Hz), 33.6, 31.8, 29.6. $^{31}P\{^1H\}$ NMR (MHz, C_6D_6): δ 24.6. Anal. Calcd for $C_{28}H_{62}Cl_2P_2Pd$: C, 52.71; H, 9.79; Cl, 11.11. Found: C, 52.98; H, 9.81; Cl, 10.79.

$(PNp_3)_2PdCl_2$ (2c).[43] $(CH_3CN)_2PdCl_2$ (50 mg, 0.2 mmol) and PNp_3 (98 mg, 0.4 mmol) were reacted following the general method to yield 97.9 mg (73%) of the product as a yellow solid. ^1H NMR (500 MHz, $CDCl_3$): δ 2.20 (t, J_{P-H} = 3.6 Hz, 12H), 1.26 (s, 54H). ^{13}C NMR (125 MHz, $CDCl_3$): δ 37.3 (t, J_{P-C} = 9.4 Hz), 33.1 (t, J_{P-C} = 2.8 Hz), 32.5. $^{31}P\{^1H\}$ NMR (202.5 MHz, $CDCl_3$): δ 3.2. Anal. Calcd for $C_{30}H_{66}Cl_2P_2Pd$: C, 54.09; H, 9.99; Cl, 10.64. Found: C, 54.52; H, 10.20; Cl, 10.29.

Synthesis of $(P(t\text{-}Bu)Np_2)PdCl_2$(4-picoline) (3b). Compound **1b** (70 mg, 0.09 mmol) was added to a vial and dissolved in 1 mL of DCM to give an orange solution. 4-Picoline (17 μL, 0.18 mmol) was added to the solution, and an immediate color change to yellow was observed. Conversion to product was determined by ^{31}P NMR spectroscopy. X-ray quality crystals were obtained by cooling a concentrated solution of product in DCM with an excess of 4-picoline (10 equiv). Proton and phosphorus NMR spectra were obtained by dissolving a crystal in $CDCl_3$. ^1H NMR (500 MHz, $CDCl_3$): δ 8.92 (m, 2H), 6.34 (d, J = 5.8 Hz, 2H), 2.55 (dd, J = 15.0 Hz, 12.2 Hz, 2H), 1.79 (dd, J = 14.8 Hz, 12.8 Hz, 2H), 1.67 (s, 18H), 1.57 (d, J = 14 Hz, 9H), 1.57 (s, 3H). $^{31}P\{^1H\}$ NMR (202.5 MHz, $CDCl_3$): δ 36.1.

General Method for ^{31}P NMR Spectroscopy Equilibrium Experiments. All solutions were prepared in the drybox in oven-dried volumetric glassware. For all experiments, standard solutions of known concentration were first prepared for each component of the mixture. Trimethyl phosphate was used as an internal standard. For all experiments, a 0.13 M solution of trimethyl phosphate was freshly prepared by adding 15 μL of trimethyl phosphate to a 1 mL volumetric flask and was diluted to the mark with corresponding solvent ($CDCl_3$ or C_6D_6). In all experiments, a 0.026 M solution of

https://dx.doi.org/10.1021/acs.inorgchem.0c00266
Inorg. Chem. 2020, 59, 5579−5592

$[(R_3P)Pd(\mu\text{-}Cl)Cl]_2$ was prepared. For experiments using P(*t*-Bu)$_2$Np and PNp$_3$ 1 M solutions of free ligand were prepared. And for experiments using P(*t*-Bu)Np$_2$, 0.1 M solutions were prepared. For all experiments, 100 μL of 0.13 M trimethyl phosphate and 500 μL of 0.026 M $[(R_3P)Pd(\mu\text{-}Cl)Cl]_2$ were first added to an empty 1 mL volumetric flask. For each set of experiments, four solutions were prepared with constant initial concentrations of trimethyl phosphate and $[(R_3P)Pd(\mu\text{-}Cl)Cl]_2$ and varied initial concentrations of free ligand (Table S2, Supporting Information). The resulting solutions analyzed by $^{31}P\{^1H\}$ NMR using an inverse-gated, proton-phosphorus decoupled pulse program setting the delay time to 3 × T1 for each ligand. Inversion recovery experiments were used for each ligand to determine the ^{31}P T1 value as described in the Supporting Information (Table S1).

Computational Methods. The geometries were optimized at the density functional level[44] with two different functionals, BP86[22] and SVWN5.[23] The calculations used the DZVP2[45] basis set for the first and second row atoms (H, C, N, P) and the pseudopotential (PP) based aug-cc-pVDZ-PP correlation-consistent basis set for Pd.[46] Vibrational frequencies were calculated to ensure that the optimized structures were minima. Additional single point calculation using the same basis sets and BP86 optimized geometries were done using the B3LYP exchange-correlation functional,[34] M06,[37] ωB97xD,[35] CAM-B3LYP,[36] and HSEh1PBE.[39] The gas phase calculations were performed using the Gaussian 09 program system.[47] Calculations in $CHCl_3$ (ε = 4.71), C_6H_6 (ε = 2.27), THF (ε = 7.43), and DMSO (ε = 46.83) solutions were performed using a self-consistent reaction field approach (SCRF)[48] with the COSMO parameters[49] using Gaussian 03.[50] The Gibbs free energy in solution (ΔG_{sol}) at 298 K was calculated from eq 5:

$$\Delta G_{sol} = \Delta G_{gas} + \Delta G_{solv} \quad (5)$$

where ΔG_{gas} is the gas phase free energy at 298 K and ΔG_{solv} is the solvation free energy at 298 K. The solvation energy is the electrostatic term (polarized solute − solvent). The SVWN5 geometries were used to predict the ^{31}P NMR chemical shifts in the gas phase and in $CHCl_3$ solvent using the ADF program system[51] with the BP86 as a functional and the TZ2P basis sets implemented in ADF using the GIAO approach.[52] Scalar relativistic effects were included at the two-component zero-order regular approximation (ZORA) level for the NMR calculations.[53] The ^{31}P NMR chemical shifts are reported relative to H_3PO_4 as standard calculated at the same level.

■ ASSOCIATED CONTENT

Supporting Information

The Supporting Information is available free of charge at https://pubs.acs.org/doi/10.1021/acs.inorgchem.0c00266.

> Steric contour maps of crystallographic and calculated structures, calculated ^{31}P NMR shifts for complexes **1** and **2**, details of phosphine binding equilibria studies, NMR spectra of isolated complexes, X-ray crystallography data, additional reaction energies, and Cartesian coordinates in Ångstroms for optimized DFT geometries (PDF)

Accession Codes

CCDC 1978595−1978601 contain the supplementary crystallographic data for this paper. These data can be obtained free of charge via www.ccdc.cam.ac.uk/data_request/cif, by emailing data_request@ccdc.cam.ac.uk, or by contacting The Cambridge Crystallographic Data Centre, 12 Union Road, Cambridge CB2 1EZ, UK; fax: + 44 1223 336033.

■ AUTHOR INFORMATION

Corresponding Authors

David A. Dixon − *Department of Chemistry and Biochemistry, The University of Alabama, Tuscaloosa, Alabama 35487-0336, United States;* orcid.org/0000-0002-9492-0056; Email: dadixon@ua.edu

Kevin H. Shaughnessy − *Department of Chemistry and Biochemistry, The University of Alabama, Tuscaloosa, Alabama 35487-0336, United States;* orcid.org/0000-0002-1375-5563; Email: kshaughn@ua.edu

Authors

Kerry L. Barnett − *Department of Chemistry and Biochemistry, The University of Alabama, Tuscaloosa, Alabama 35487-0336, United States*

Monica Vasiliu − *Department of Chemistry and Biochemistry, The University of Alabama, Tuscaloosa, Alabama 35487-0336, United States;* orcid.org/0000-0001-7573-4787

Trent H. Stein − *Department of Chemistry and Biochemistry, The University of Alabama, Tuscaloosa, Alabama 35487-0336, United States*

Matthew V. Delahay − *Department of Chemistry and Biochemistry, The University of Alabama, Tuscaloosa, Alabama 35487-0336, United States*

Fengrui Qu − *Department of Chemistry and Biochemistry, The University of Alabama, Tuscaloosa, Alabama 35487-0336, United States;* orcid.org/0000-0002-9975-2573

Deidra L. Gerlach − *Department of Chemistry and Biochemistry, The University of Alabama, Tuscaloosa, Alabama 35487-0336, United States*

Complete contact information is available at: https://pubs.acs.org/10.1021/acs.inorgchem.0c00266

Notes

The authors declare no competing financial interest.

■ ACKNOWLEDGMENTS

Acknowledgment is made to the National Science Foundation (CHE-1058984) for partial financial support of the experimental work. The structures of both polymorphs of **1a** were obtained on an X-ray diffractometer purchased with support from the NSF MRI program (CHE MRI 1828078). Johnson-Matthey is acknowledged for donation of palladium salts. The computational work was supported by the Chemical Sciences, Geosciences and Biosciences Division, Office of Basic Energy Sciences, U.S. Department of Energy (DOE) under the Catalysis Center Program by a subcontract from the Pacific Northwest National Laboratory (KC0301050-47319). D.A.D. also thanks the Robert Ramsay Chair Fund of The University of Alabama for support. K.L.B. acknowledges support from a GAANN fellowship (DoEd, P200A150329).

■ REFERENCES

(1) (a) White, D.; Coville, N. J. Quantification of Steric Effects in Organometallic Chemistry. In *Adv. Organomet. Chem.*, Stone, F. G. A., West, R., Eds.; Academic Press, Inc: San Diego, CA, 1994; Vol. *36*, pp 95−158. (b) Fey, N.; Orpen, A. G.; Harvey, J. N. Building Ligand Knowledge Bases for Organometallic Chemistry: Computational Description of Phosphorus(Iii)-Donor Ligands and the Metal-Phosphorus Bond. *Coord. Chem. Rev.* **2009**, *253*, 704−722. (c) Bilbrey, J. A.; Allen, W. D. Ligand Steric Descriptors. In *Annual Reports in Computational Chemistry*; Wheeler, R., Ed.; Elsevier B. V.: Amsterdam, Netherlands, 2013; Vol. *9*, pp 3−23.

(2) (a) Tolman, C. A. Phosphorous Ligand Exchange Equilibria on Zerovalent Nickel. A Dominant Role for Steric Effects. *J. Am. Chem. Soc.* **1970**, *92*, 2956−2965. (b) Tolman, C. A. Steric Effects of Phosphorous Ligands in Organometallic Chemistry and Homogenous Catalysis. *Chem. Rev.* **1977**, *77*, 313−348.
(3) Bilbrey, J. A.; Kazez, A. H.; Locklin, J.; Allen, W. D. Exact Ligand Cone Angles. *J. Comput. Chem.* **2013**, *34*, 1189−1197.
(4) (a) Immirzi, A.; Musco, A. A Method to Measure the Size of Phosphorus Ligands in Coordination Complexes. *Inorg. Chim. Acta* **1977**, *25*, L41−L42. (b) Taverner, B. C. Improved Algorithm for Accurate Computation of Molecular Solid Angles. *J. Comput. Chem.* **1996**, *17*, 1612−1623.
(5) (a) Hillier, A. C.; Sommer, W. J.; Yong, B. S.; Petersen, J. L.; Cavallo, L.; Nolan, S. P. A Combined Experimental and Theoretical Study Examining the Binding of N-Heterocyclic Carbenes (NHC) to the Cp*RuCl (Cp* = η^5-C_5Me_5) Moiety: Insight into Stereoelectronic Differences between Unsaturated and Saturated NHC Ligands. *Organometallics* **2003**, *22*, 4322−4326. (b) Poater, A.; Cosenza, B.; Correa, A.; Giudice, S.; Ragone, F.; Scarano, V.; Cavallo, L. Samb*V* ca: A Web Application for the Calculation of the Buried Volume of *N*-Heterocyclic Carbene Ligands. *Eur. J. Inorg. Chem.* **2009**, *2009*, 1759−1766. (c) Falivene, L.; Credendino, R.; Poater, A.; Petta, A.; Serra, L.; Oliva, R.; Scarano, V.; Cavallo, L. SambVca 2. A Web Tool for Analyzing Catalytic Pockets with Topographic Steric Maps. *Organometallics* **2016**, *35*, 2286−2293. (d) Falivene, L.; Cao, Z.; Petta, A.; Serra, L.; Poater, A.; Oliva, R.; Scarano, V.; Cavallo, L. Towards the Online Computer-Aided Design of Catalytic Pockets. *Nat. Chem.* **2019**, *11*, 872−879.
(6) Dunne, B. J.; Morris, R. B.; Orpen, A. G. Structural Systematics. Part 3. Geometry Deformations in Triphenylphosphine Fragments: a Test of Bonding Theories in Phosphine Complexes. *J. Chem. Soc., Dalton Trans.* **1991**, 653−661.
(7) Kendall, A. J.; Zakharov, L. N.; Tyler, D. R. Steric and Electronic Influences of Buchwald-Type Alkyl-JohnPhos Ligands. *Inorg. Chem.* **2016**, *55*, 3079−3090.
(8) Tolman, C. A. Electron Donor-Acceptor Properties of Phosphorous Ligands. Substituent Activity. *J. Am. Chem. Soc.* **1970**, *92*, 2953−2956.
(9) (a) Stelzer, O.; Unger, E. σ-Donor- and π-Acceptor Properties of the Phosphine Ligands in Complexes of the Type *cis*-$Mo(CO)_4(R_{3-n})PX_n)_2$. *Chem. Ber.* **1975**, *108*, 1246−1258. (b) Barbeau, C.; Turcotte, J. Donor and Acceptor Powers of Ligands from Derivatives of $Mo(CO)_6$. *Can. J. Chem.* **1976**, *54*, 1603−1611. (c) Vastag, S.; Heil, B.; Markó, L. Effect of Phosphine Structure on Catalytic Activity in Acetone Hydrogenation. *J. Mol. Catal.* **1979**, *5*, 189−195. (d) Chianese, A. R.; Li, X.; Janzen, M. C.; Faller, J. W.; Crabtree, R. H. Rhodium and Iridium Complexes of N-Heterocyclic Carbenes via Transmetalation: Structure and Dynamics. *Organometallics* **2003**, *22*, 1663−1667. (e) Kelly, R. A., III; Clavier, H.; Giudice, S.; Scott, N. M.; Stevens, E. D.; Bordner, J.; Samardjiev, I.; Hoff, C. D.; Cavallo, L.; Nolan, S. P. Determination of N-Heterocyclic Carbene (NHC) Steric and Electronic Parameters Using the [(NHC)Ir$(CO)_2$Cl] System. *Organometallics* **2008**, *27*, 202−210. (f) Wolf, S.; Plenio, H. Synthesis of (NHC)Rh(cod)Cl and (NHC)Rh$Cl(CO)_2$ Complexes − Translation of the Rh- into the Ir-Scale for the Electronic Properties of Nhc Ligands. *J. Organomet. Chem.* **2009**, *694*, 1487−1492.
(10) (a) Fey, N.; Tsipis, A. C.; Harris, S. E.; Harvey, J. N.; Orpen, A. G.; Mansson, R. A. Development of a Ligand Knowledge Base, Part 1: Computational Descriptors for Phosphorus Donor Ligands. *Chem. - Eur. J.* **2006**, *12*, 291−302. (b) Jover, J.; Fey, N.; Harvey, J. N.; Lloyd-Jones, G. C.; Orpen, A. G.; Owen-Smith, G. J. J.; Murray, P.; Hose, D. R. J.; Osborne, R.; Purdie, M. Expansion of the Ligand Knowledge Base for Monodentate P-Donor Ligands (LKB-P). *Organometallics* **2010**, *29*, 6245−6258.
(11) (a) Hill, L. L.; Moore, L. R.; Huang, R.; Craciun, R.; Vincent, A. J.; Dixon, D. A.; Chou, J.; Woltermann, C. J.; Shaughnessy, K. H. Bulky Alkylphosphines with Neopentyl Substituents as Ligands in the Amination of Aryl Bromides and Chlorides. *J. Org. Chem.* **2006**, *71*, 5117−5125. (b) Hill, L. L.; Smith, J. M.; Brown, W. S.; Moore, L. R.; Guevera, P.; Pair, E. S.; Porter, J.; Chou, J.; Wolterman, C. J.; Craciun, R.; Dixon, D. A.; Shaughnessy, K. H. Neopentylphosphines as Effective Ligands in Palladium-Catalyzed Cross-Couplings of Aryl Bromides and Chlorides. *Tetrahedron* **2008**, *64*, 6920−6934. (c) Hill, L. L.; Crowell, J. L.; Tutwiler, S. L.; Massie, N. L.; Hines, C. C.; Griffin, S. T.; Rogers, R. D.; Shaughnessy, K. H.; Grasa, G. A.; Johansson Seechurn, C. C. C.; Li, H.; Colacot, T. J.; Chou, J.; Woltermann, C. J. Synthesis and X-Ray Structure Determination of Highly Active Pd(II), Pd(I) and Pd(0) Complexes of Di-(*tert*-butyl)neopentylphosphine (DTBNpP) in the Arylation of Amines and Ketones. *J. Org. Chem.* **2010**, *75*, 6477−6488. (d) Raders, S. M.; Jones, J. M.; Semmes, J. G.; Kelley, S. P.; Rogers, R. D.; Shaughnessy, K. H. Di-*tert*-Butylneopentylphosphine (DTBNpP): An Efficient Ligand in the Palladium-Catalyzed A-Arylation of Ketones. *Eur. J. Org. Chem.* **2014**, *2014*, 7395−7404. (e) Semmes, J. G.; Bevans, S. L.; Mullins, H. C.; Shaughnessy, K. H. Arylation of Diethyl Malonate and Ethyl Cyanoacetate Catalyzed by Palladium/Di-Tert-Butylneopentylphosphine. *Tetrahedron Lett.* **2015**, *56*, 3447−3450. (f) Barnett, K. L.; Howard, J. R.; Treager, C. J.; Shipley, A. T.; Stullich, R. M.; Qu, F.; Gerlach, D. L.; Shaughnessy, K. H. Air-Stable $[(R_3P)PdCl_2]_2$ Complexes of Neopentylphosphines as Cross-Coupling Precatalysts: Catalytic Application and Mechanism of Catalyst Activation and Deactivation. *Organometallics* **2018**, *37*, 1410−1424.
(12) Lauer, M. G.; Thompson, M. K.; Shaughnessy, K. H. Controlling Olefin Isomerization in the Heck Reaction with Neopentyl Phosphine Ligands. *J. Org. Chem.* **2014**, *79*, 10837−10848.
(13) (a) Raders, S. M.; Moore, J. N.; Parks, J. K.; Miller, A. D.; Leißing, T. M.; Kelley, S. P.; Rogers, R. D.; Shaughnessy, K. H. Trineopentylphosphine: A Conformationally Flexible Ligand for the Coupling of Sterically Demanding Substrates in the Buchwald-Hartwig Amination and Suzuki-Miyaura Reaction. *J. Org. Chem.* **2013**, *78*, 4649−4664. (b) Hu, H.; Qu, F.; Gerlach, D. L.; Shaughnessy, K. H. Mechanistic Study of the Role of Substrate Steric Effects and Aniline Inhibition on the Bis(trineopentylphosphine)palladium(0)-Catalyzed Arylation of Aniline Derivatives. *ACS Catal.* **2017**, *7*, 2516−2527.
(14) Hu, H.; Vasiliu, M.; Stein, T. H.; Qu, F.; Gerlach, D. L.; Dixon, D. A.; Shaughnessy, K. H. Synthesis, Structural Characterization, and Coordination Chemistry of (Trineopentylphosphine)palladium(aryl)-bromide Dimer Complexes ($[(Np_3P)Pd(Ar)Br]_2$). *Inorg. Chem.* **2019**, *58*, 13299−13313.
(15) (a) Smith, J. M.; Coville, N. J.; Cook, L. M.; Boeyens, J. C. A. Steric Parameters of Conformationally Flexible Ligands from X-ray Structural Data. 1. $P(OR)_3$ Ligands in Equivalent Ligand Environments. *Organometallics* **2000**, *19*, 5273−5280. (b) Bunten, K. A.; Chen, L.; Fernandez, A. L.; Poë, A. J. Cone angles: Tolman′s and Plato′s. *Coord. Chem. Rev.* **2002**, *233*−*234*, 41−51.
(16) Smith, J. M.; Coville, N. J. Steric Parameters of Conformationally Flexible Ligands from X-ray Structural Data. 2. $P(OR)_3$ Ligands in Multiple Ligand Environments. *Organometallics* **2001**, *20*, 1210−1215.
(17) Goel, R. G.; Ogini, W. O. Some Novel Reactions of Tri-*tert*-butylphosphine with Iridium(III), Rhodium(III), Platinum(II), and Palladium(II) Chlorides. *Organometallics* **1982**, *1*, 654−658.
(18) Viñas, C.; Cirera, M. R.; Teixidor, F.; Kivekäs, R.; Sillanpää, R.; Llibre, J. Synthesis and Characterization of the First Cyclic Monothioether Derivative of 1,2-*o*-Carborane and Its Reactivity toward Phosphine Transition Metal Complexes. *Inorg. Chem.* **1998**, *37*, 6746−6750.
(19) Grim, S. O.; Keiter, R. L. Phosphorus-31 Magnetic Resonance Study of Tertiary Phosphine Palladium(II) Compounds. *Inorg. Chim. Acta* **1970**, *4*, 56−60.
(20) Moore, L. R.; Western, E. C.; Craciun, R.; Spruell, J. M.; Dixon, D. A.; O′Halloran, K. P.; Shaughnessy, K. H. Sterically Demanding, Sulfonated, Triarylphosphines: Application to Palladium-Catalyzed Cross-Coupling, Steric and Electronic Properties, and Coordination Chemistry. *Organometallics* **2008**, *27*, 576−593.
(21) Hill, L. L. *Investigations of Cross Coupling Reactions: Synthesis and Scope of New Neopentyl Phosphine Ligands and Pre-Formed*

https://dx.doi.org/10.1021/acs.inorgchem.0c00266
Inorg. Chem. 2020, 59, 5579−5592

Palladium Catalysts. Ph.D. Thesis, The University of Alabama, Tuscaloosa, AL, 2009.
(22) (a) Becke, A. D. Density-Functional Exchange-Energy Approximation with Correct Asymptotic Behavior. *Phys. Rev. A: At., Mol., Opt. Phys.* **1988**, *38*, 3098−3100. (b) Perdew, J. P. Density-functional approximation for the correlation energy of the inhomogeneous electron gas. *Phys. Rev. B: Condens. Matter Mater. Phys.* **1986**, *33*, 8822−8824.
(23) (a) Slater, J. C. *The Self-Consistent Field for Molecular and Solids, Quantum Theory of Molecular and Solids*; McGraw-Hill: New York, NY, 1974; p 583. (b) Vosko, S. H.; Wilk, L.; Nusair, M. Accurate Spin-Dependent Electron Liquid Correlation Energies for Local Spin Density Calculations: a Critical Analysis. *Can. J. Phys.* **1980**, *58*, 1200−1211.
(24) Hills, I. D.; Fu, G. C. Elucidating Reactivity Differences in Palladium-Catalyzed Coupling Processes: The Chemistry of Palladium Hydrides. *J. Am. Chem. Soc.* **2004**, *126*, 13178−13179.
(25) (a) Yang, L.; Powell, D. R.; Houser, R. P. Structural Variation in Copper(I) Complexes with Pyridylmethylamide Ligands: Structural Analysis with a New Four-Coordinate Geometry Index, τ4. *Dalton Trans.* **2007**, 955−964. (b) Okuniewski, A.; Rosiak, D.; Chojnacki, J.; Becker, B. Coordination Polymers and Molecular Structures Among Complexes of Mercury(II) Halides with Selected 1-Benzoylthioureas. *Polyhedron* **2015**, *90*, 47−57.
(26) (a) Clark, H. C.; Ferguson, G.; Jain, V. K.; Parvez, M. Preparation and Characterization of Heterobimetallic Halogen-Bridged Palladium-Platinum Complexes. Crystal and Molecular Structure of $[(PEt_3)ClPd(\mu\text{-}Cl)_2PtCl(PEt_3)]$. *Inorg. Chem.* **1985**, *24*, 1477−1482. (b) Chaloner, P. A.; Dewa, S. Z.; Hitchcock, P. B. *trans*-Di-μ-chloro-bis[chloro(tributylphosphine)palladium]. *Acta Crystallogr., Sect. C: Cryst. Struct. Commun.* **1995**, *51*, 232−233. (c) Stein, T.; Hoffman, F.; Fröba, M., Bis(triethylphosphine)palladium Dichloride. *CSD Commun.*; CCDC, 2016; p 1485811.
(27) (a) Orpen, A. G.; Connelly, N. G. Structural Systematics: Role of P-A σ* Orbitals in Metal-Phosphorus π-Bonding in Redox-Related Pairs of M-PA_3 Complexes (A = R, Ar, OR; R = Alkyl). *Organometallics* **1990**, *9*, 1206−1210. (b) Leyssens, T.; Peeters, D.; Orpen, A. G.; Harvey, J. N. Insight into Metal-Phosphorus Bonding from Analysis of the Electronic Structure of Redox Pairs of Metal-Phosphine Complexes. *New J. Chem.* **2005**, *29*, 1424−1430.
(28) Bruckmann, J.; Kruger, C. Trimethylphosphine and Triethylphosphine in the Solid State. *Acta Crystallogr., Sect. C: Cryst. Struct. Commun.* **1995**, *51*, 1155−1158.
(29) Tanaka, M. Structure of Bis(tri-*tert*-butylphosphine)palladium-(0). *Acta Crystallogr., Sect. C: Cryst. Struct. Commun.* **1992**, *C48*, 739−40.
(30) Curtiss, L. A.; Redfern, P. C.; Raghavachari, K.; Rassolov, V.; Pople, J. A. Gaussian-3 Theory Using Reduced Møller-Plesset Order. *J. Chem. Phys.* **1999**, *110*, 4703−4709.
(31) Hunter, E. P. L.; Lias, S. G. Evaluated Gas Phase Basicities and Proton Affinities of Molecules: An Update. *J. Phys. Chem. Ref. Data* **1998**, *27*, 413−656.
(32) (a) Dixon, D. A.; Feller, D.; Peterson, K. A. Practical Guide to Reliable First Principles Computational Thermochemistry Predictions across the Periodic Table. In *Annual Reports in Computational Chemistry*; Wheeler, R. A., Ed.; Elsevier B.V.: Amsterdam, Netherlands, 2012; Vol. *8*, pp 1−28. (b) Peterson, K. A.; Feller, D.; Dixon, D. A. Chemical accuracy in ab initio thermochemistry and spectroscopy: current strategies and future challenges. *Theor. Chem. Acc.* **2012**, *131*, 1079. (c) Feller, D.; Peterson, K. A.; Dixon, D. A. Further Benchmarks of a Composite, Convergent, Statistically Calibrated Coupled-Cluster-Based Approach for Thermochemical and Spectroscopic Studies. *Mol. Phys.* **2012**, *110*, 2381−2399. (d) Feller, D.; Peterson, K. A.; Dixon, D. A. The Impact of Larger Basis Sets and Explicitly Correlated Coupled Cluster Theory on the Feller-Peterson-Dixon Composite Method. In *Annual Reports in Computational Chemistry*; Dixon, D. A., Ed.; Elsevier: Amsterdam, Netherlands, 2016; Vol. *12*, pp 47−78.
(33) (a) Craciun, R.; Vincent, A. J.; Shaughnessy, K. H.; Dixon, D. A. Prediction of Reliable Metal-PH_3 Bond Energies for Ni, Pd, and Pt in the 0 and + 2 Oxidation States. *Inorg. Chem.* **2010**, *49*, 5546−5553. (b) Craciun, R.; Vincent, A. J.; Shaughnessy, K. H.; Dixon, D. A. Correction to Prediction of Reliable Metal−PH_3 Bond Energies for Ni, Pd, and Pt in the 0 and + 2 Oxidation States. *Inorg. Chem.* **2011**, *50*, 5307.
(34) (a) Becke, A. D. Density Functional Thermochemistry. Iii. The Role of Exact Exchange. *J. Chem. Phys.* **1993**, *98*, 5648−5652. (b) Lee, C.; Yang, W.; Parr, R. G. Development of the Colle-Salvetti correlation-energy formula into a functional of the electron density. *Phys. Rev. B: Condens. Matter Mater. Phys.* **1988**, *37*, 785−789.
(35) Chai, J.-D.; Head-Gordon, M. Long-Range Corrected Hybrid Density Functionals with Damped Atom-Atom Dispersion Corrections. *Phys. Chem. Chem. Phys.* **2008**, *10*, 6615−6620.
(36) Yanai, T.; Tew, D. P.; Handy, N. C. A New Hybrid Exchange−Correlation Functional Using the Coulomb-Attenuating Method (CAM-B3LYP). *Chem. Phys. Lett.* **2004**, *393*, 51−57.
(37) Zhao, Y.; Truhlar, D. G. The M06 Suite of Density Functionals for Main Group Thermochemistry, Thermochemical Kinetics, Noncovalent Interactions, Excited States, and Transition Elements: Two New Functionals and Systematic Testing of Four M06-Class Functionals and 12 Other Functionals. *Theor. Chem. Acc.* **2008**, *120*, 215−241.
(38) (a) Tao, J.; Perdew, J. P.; Staroverov, V. N.; Scuseria, G. E. Climbing the Density Functional Ladder: Nonempirical Meta−Generalized Gradient Approximation Designed for Molecules and Solids. *Phys. Rev. Lett.* **2003**, *91*, 146401. (b) Staroverov, V. N.; Scuseria, G. E.; Tao, J.; Perdew, J. P. Comparative Assessment of a New Nonempirical Density Functional: Molecules and Hydrogen-Bonded Complexes. *J. Chem. Phys.* **2003**, *119*, 12129−12137.
(39) (a) Heyd, J.; Scuseria, G. E.; Ernzerhof, M. Hybrid Functionals Based on a Screened Coulomb Potential. *J. Chem. Phys.* **2003**, *118*, 8207−8215. (b) Heyd, J.; Scuseria, G. E. Efficient Hybrid Density Functional Calculations in Solids: Assessment of the Heyd−Scuseria−Ernzerhof Screened Coulomb Hybrid Functional. *J. Chem. Phys.* **2004**, *121*, 1187−1192. (c) Heyd, J.; Scuseria, G. E. Assessment and Validation of a Screened Coulomb Hybrid Density Functional. *J. Chem. Phys.* **2004**, *120*, 7274−7280. (d) Heyd, J.; Peralta, J. E.; Scuseria, G. E.; Martin, R. L. Energy Band Gaps and Lattice Parameters Evaluated with the Heyd-Scuseria-Ernzerhof Screened Hybrid Functional. *J. Chem. Phys.* **2005**, *123*, 174101. (e) Henderson, T. M.; Izmaylov, A. F.; Scalmani, G.; Scuseria, G. E. Can Short-Range Hybrids Describe Long-Range-Dependent Properties? *J. Chem. Phys.* **2009**, *131*, 044108. (f) Izmaylov, A. F.; Scuseria, G. E.; Frisch, M. J. Efficient Evaluation of Short-Range Hartree-Fock Exchange in Large Molecules and Periodic Systems. *J. Chem. Phys.* **2006**, *125*, 104103. (g) Krukau, A.; Vydrov, O. A.; Izmaylov, A. F.; Scuseria, G. E. Influence of the Exchange Screening Parameter on the Performance of Screened Hybrid Functionals. *J. Chem. Phys.* **2006**, *125*, 224106.
(40) Jover, J.; Cirera, J. Computational Assessment on the Tolman Cone Angles for P-Ligands. *Dalton Trans.* **2019**, *48*, 15036−15048.
(41) (a) Stambuli, J. P.; Bühl, M.; Hartwig, J. F. Synthesis, characterization, and reactivity of monomeric arylpalladium halide complexes with a hindered phosphine as the only dative ligand. *J. Am. Chem. Soc.* **2002**, *124*, 9346−9347. (b) Stambuli, J. P.; Incarvito, C. D.; Bühl, M.; Hartwig, J. F. Synthesis, structure, theoretical studies, and ligand exchange reactions of monomeric, T-shaped arylpalladium-(II) halide complexes with an additional, weak agostic interaction. *J. Am. Chem. Soc.* **2004**, *126*, 1184−1194.
(42) King, R. B.; Cloyd, J. C., Jr.; Reimann, R. H. Poly(Tertiary Phosphines and Arsines). XIII. Some Neopentyl Poly(Tertiary Phosphines). *J. Org. Chem.* **1976**, *41*, 972−977.
(43) King, R. B.; Cloyd, J. C., Jr.; Norins, M. E.; Reimann, R. H. Complexes of Trivalent Phosphorus Derivatives, XVIII. Some Complexes of Neopentylphosphines with Rhodium, Nickel, and Palladium Chlorides. *J. Coord. Chem.* **1977**, *7*, 23−26.
(44) Parr, R. G.; Yang, W. *Density Functional Theory of Atoms and Molecules*; Springer-Verlag: New York, 1989.

https://dx.doi.org/10.1021/acs.inorgchem.0c00266
Inorg. Chem. 2020, 59, 5579−5592

(45) Godbout, N.; Salahub, D. R.; Andzelm, J.; Wimmer, E. Optimization of Gaussian-Type Basis Sets for Local Spin Density Functional Calculations. Part I. Boron Through Neon, Optimization Technique and Validation. *Can. J. Chem.* **1992**, *70*, 560−571.
(46) (a) Peterson, K. A.; Figgen, D.; Dolg, M.; Stoll, H. Energy-consistent relativistic pseudopotentials and correlation consistent basis sets for the 4d elements Y−Pd. *J. Chem. Phys.* **2007**, *126*, 124101. (b) Figgen, D.; Peterson, K. A.; Dolg, M.; Stoll, H. Energy-Consistent Pseudopotentials and Correlation Consistent Basis Sets for the 5d Elements Hf−Pt. *J. Chem. Phys.* **2009**, *130*, 164108.
(47) Frisch, M. J.; Trucks, G. W.; Schlegel, H. B.; Scuseria, G. E.; Robb, M. A.; Cheeseman, J. R.; Scalmani, G.; Barone, V.; Mennucci, B.; Petersson, G. A.; Nakatsuji, H.; Caricato, M.; Li, X.; Hratchian, H. P.; Izmaylov, A. F.; Bloino, J.; Zheng, G.; Sonnenberg, J. L.; Hada, M.; Ehara, M.; Toyota, K.; Fukuda, R.; Hasegawa, J.; Ishida, M.; Nakajima, T.; Honda, Y.; Kitao, O.; Nakai, H.; Vreven, T.; Montgomery, J. A., Jr.; Peralta, J. E.; Ogliaro, F.; Bearpark, M.; Heyd, J. J.; Brothers, E.; Kudin, K. N.; Staroverov, V. N.; Kobayashi, R.; Normand, J.; Raghavachari, K.; Rendell, A.; Burant, J. C.; Iyengar, S. S.; Tomasi, J.; Cossi, M.; Rega, N.; Millam, J. M.; Klene, M.; Knox, J. E.; Cross, J. B.; Bakken, V.; Adamo, C.; Jaramillo, J.; Gomperts, R.; Stratmann, R. E.; Yazyev, O.; Austin, A. J.; Cammi, R.; Pomelli, C.; Ochterski, J. W.; Martin, R. L.; Morokuma, K.; Zakrzewski, V. G.; Voth, G. A.; Salvador, P.; Dannenberg, J. J.; Dapprich, S.; Daniels, A. D.; Farkas, Ö.; Foresman, J. B.; Ortiz, J. V.; Cioslowski, J.; Fox, D. J. *Gaussian 09*, revision E.01; Gaussian, Inc: Wallingford, CT, 2009.
(48) Tomasi, J.; Mennucci, B.; Cammi, R. Quantum Mechanical Continuum Solvation Models. *Chem. Rev.* **2005**, *105*, 2999−3093.
(49) (a) Klamt, A. *COSMO-RS. From Quantum Chemistry to Fluid Phase Thermodynamics and Drug Design*; Elsevier: Amsterdam, Netherlands, 2005; p 218. (b) Klamt, A.; Schüürmann, G. COSMO: A New Approach to Dielectric Screening in Solvents with Explicit Expressions for the Screening Energy and its Gradient. *J. Chem. Soc., Perkin Trans. 2* **1993**, 799−805.
(50) Frisch, M. J.; Trucks, G. W.; Schlegel, H. B.; Scuseria, G. E.; Robb, M. A.; Cheeseman, J. R.; Montgomery, J. A., Jr.; Vreven, T.; Kudin, K. N.; Burant, J. C.; Millam, J. M.; Iyengar, S. S.; Tomasi, J.; Barone, V.; Mennucci, B.; Cossi, M.; Scalmani, G.; Rega, N.; Petersson, G. A.; Nakatsuji, H.; Hada, M.; Ehara, M.; Toyota, K.; Fukuda, R.; Hasegawa, J.; Ishida, M.; Nakajima, T.; Honda, Y. K. O.; Nakai, H.; Klene, M.; Li, X.; Knox, J. E.; Hratchian, H. P.; Cross, J. B.; Bakken, V.; Adamo, C.; Jaramillo, J.; Gomperts, R.; Stratmann, R. E.; Yazyev, O.; Austin, A. J.; Cammi, R.; Pomelli, C.; Ochterski, J. W.; Ayala, P. Y.; Morokuma, K.; Voth, G. A.; Salvador, P.; Dannenberg, J. J.; Zakrzewski, V. G.; Dapprich, S.; Daniels, A. D.; Strain, M. C.; Farkas, O.; Malick, D. K.; Rabuck, A. D.; Raghavachari, K.; Foresman, J. B.; Ortiz, J. V.; Cui, Q.; Baboul, A. G.; Clifford, S.; Cioslowski, J.; Stefanov, B. B.; Liu, G.; Liashenko, A.; Piskorz, P.; Komaromi, I.; Martin, R. L.; Fox, D. J.; Keith, T.; Al-Laham, M. A.; Peng, C. Y.; Nanayakkara, A.; Challacombe, M.; Gill, P. M. W.; Johnson, B.; Chen, W.; Wong, M. W.; Gonzalez, C.; Pople, J. A. *Gaussian 03*, revision E.01; revision C.02; Gaussian Inc: Wallingford, CT, 2004.
(51) (a) te Velde, G.; Bickelhaupt, F. M.; Baerends, E. J.; Fonseca Guerra, C.; van Gisbergen, J. A.; Snijders, J. G.; Ziegler, T. Chemsitry with ADF. *J. Comput. Chem.* **2001**, *22*, 931−967. (b) *ADF 2008.01*; SCM, Theoretical Chemistry; Vrije Universiteit: Amsterdam, 2008.
(52) Wolinski, K.; Hinton, J. F.; Pulay, P. Efficient Implementation of the Guage-Independent Atomic Orbital Method for NMR Chemical Shift Calculation. *J. Am. Chem. Soc.* **1990**, *112*, 8251−8260.
(53) (a) Wolff, S. K.; Ziegler, T.; van Lenthe, E.; Baerends, E. J. Density Functional Calculations of Nuclear Magnetic Shieldings Using the Zeroth-Order Regular Approximation (Zora) for Reltivistic Effects: Zora Nuclear Magnetic Resonance. *J. Chem. Phys.* **1999**, *110*, 7689−7698. (b) van Lenthe, E.; Baerends, E. J.; Snijders, J. G. Relativistic Regular Two-Component Hamiltonians. *J. Chem. Phys.* **1993**, *99*, 4597−4610. (c) Autschbach, J.; Ziegler, T., Calculation of Heavy-Nucleus Chemical Shifts: Relativistic All-Electron Methods. In *Calculation of NMR and EPR Parameters: Theory and Application*; Kaupp, M., Buhl, M., Malkin, V. G., Eds.; Wiley-VCH & Co.: Weinheim, Germany, 2004; pp 249−264.

https://dx.doi.org/10.1021/acs.inorgchem.0c00266
Inorg. Chem. 2020, 59, 5579−5592